

A COMPARATIVE STUDY OF LOCAL GALAXY CLUSTERS: II: X-RAY AND SZ SCALING RELATIONS

EDUARDO ROZO^{1,2}, AUGUST E. EVRARD³, ELI S. RYKOFF^{4,5}, JAMES G. BARTLETT^{6,7},
Draft version September 18, 2018

ABSTRACT

We compare cluster scaling relations published for three different samples selected via X-ray and Sunyaev-Zel'dovich (SZ) signatures. We find tensions driven mainly by two factors: i) systematic differences in the X-ray cluster observables used to derive the scaling relations, and ii) uncertainty in the modeling of how the gas mass of galaxy clusters scales with total mass. All scaling relations are in agreement after accounting for these two effects. We describe a multivariate scaling model that enables a fully self-consistent treatment of multiple observational catalogs in the presence of property covariance, and apply this formalism when interpreting published results. The corrections due to scatter and observable covariance can be significant. For instance, our predicted $Y_{\text{SZ}}-L_X$ scaling relation differs from that derived using the naive “plug in” method by $\approx 25\%$. Finally, we test the mass normalization for each of the X-ray data sets we consider by applying a space density consistency test: we compare the observed REFLEX luminosity function to expectations from published L_X-M relations convolved with the mass function for a WMAP7 flat Λ CDM model.

Subject headings: cosmology; clusters

1. INTRODUCTION

The study of scaling relations of galaxy clusters is one of significant importance, both from a cosmological and an astrophysical point of view. Cosmologically, mass-observable scaling relations are a fundamental component of all work that exploits the abundance of galaxy clusters for constraining cosmological parameters (e.g. Henry et al. 2009; Vikhlinin et al. 2009a; Mantz et al. 2010a; Rozo et al. 2010). Astrophysically, the existence of a self-similar model (Kaiser 1986; Böhringer et al. 2012) allows one to use departures from this self-similar expectation as a probe of feedback and non-thermal processes in cluster and galaxy formation (e.g. Rowley et al. 2004; Magliocchetti & Brügggen 2007; Mantz et al. 2010b; Mittal et al. 2011; Maughan et al. 2012; Eckmiller et al. 2011). Likewise, the scatter of galaxy clusters about the scaling relations can also be a direct probe of the state of the intra-cluster gas (e.g. the presence or absence of a cool core) and/or dynamical state (e.g. Fabian et al. 1994; Hartley et al. 2008; Rasia et al. 2011; Krause et al. 2012). Indeed, these ideas have spurred large suites of simulations in which the physics contributing to the state of the intra-cluster gas are systematically varied, both to give a range of plausible evolution models, and to help guide theoretical interpretations of current observations (e.g. Nagai

2006; Nagai et al. 2007; Stanek et al. 2010; Short et al. 2010; Battaglia et al. 2011; Fabjan et al. 2011; Kay et al. 2012).

All this work, however, is critically dependent on our ability to robustly measure empirical cluster scaling relations. Here, we take a pragmatic approach to estimating the level of systematic differences in observed X-ray and SZ scaling relation by comparing the published values of three different sets of works: a *Planck* and *XMM* based analysis (Pratt et al. 2009; Arnaud et al. 2010; Planck Collaboration 2011b), henceforth referred simply as P11-LS, a *Chandra* and *Planck* based analysis (Vikhlinin et al. 2009a; Rozo et al. 2012a), henceforth referred to as V09, and a second, independent *Chandra* based analysis (Mantz et al. 2010b), henceforth referred to as M10. As is demonstrated below, these three works are often in tension with one another. Understanding the origins of these tensions is of paramount importance for validating the use of galaxy clusters as probes of precision cosmology.

This is the second in a series of papers that aims to perform a detailed study of local cluster scaling relations from X-ray and SZ selected clusters catalogs. In the first paper — Rozo et al. (2012b), henceforth paper I — we demonstrate significant systematic differences between different groups on raw cluster observables, including X-ray luminosity, L_X , temperature, T_X , and gas thermal energy, Y_X . More importantly, hydrostatic mass estimates vary substantially.

Paper I characterizes relative offsets in these quantities, and that information forms the foundation for the current work. Indeed, we demonstrate below that the tension in the scaling relations between the three works we consider is ultimately sourced by the systematic differences in cluster observables identified in paper I.

Having fully understood the origin of the tension between the three groups, we then proceed to derive a self-consistent set of multi-variate scaling relations from each of these data sets (see also White et al. 2010). By “self-consistent”, we mean that our propagated scal-

¹ Einstein Fellow, Department of Astronomy & Astrophysics, The University of Chicago, Chicago, IL 60637.

² Kavli Institute for Cosmological Physics, Chicago, IL 60637.

³ Departments of Physics and Astronomy and Michigan Center for Theoretical Physics, University of Michigan, Ann Arbor, MI 48109.

⁴ SLAC National Accelerator Laboratory, Menlo Park, CA 94025.

⁵ Lawrence Berkeley National Laboratory, Berkeley, CA 94720.

⁶ APC, AstroParticule et Cosmologie, Université Paris Diderot, CNRS/IN2P3, CEA/Irfu, Observatoire de Paris, Sorbonne Paris Cité, 10, rue Alice Domon et Léonie Duquet, Paris Cedex 13, France.

⁷ Jet Propulsion Laboratory, California Institute of Technology, 4800 Oak Grove Drive, Pasadena, CA, U.S.A.

ing relations are explicitly derived from a probabilistic model that account for the scatter and possible covariance between clusters observables, arising for instance from local large scale structure (e.g. White et al. 2010; Noh & Cohn 2011, 2012; Angulo et al. 2012) Most work to date relies on simple “plug-in” methods to propagate scaling relations. That is, given two scaling relations $Y(X)$ and $Z(Y)$, the $Z-X$ scaling relation is assumed to take the form $Z(Y(X))$. Recent work with numerical simulations and/or Monte Carlo analyses have made it clear, however, that this naive method is generically biased, with the error depending on both the scatter and covariance between the observables at hand (Roza et al. 2009; White et al. 2010; Biesiadzinski et al. 2012; Angulo et al. 2012). The two specific cases we consider are using the $M-Y_X$ and $Y_{SZ}-Y_X$ scaling relations to derive the $Y_{SZ}-M$ scaling relation, and using the L_X-M and $Y_{SZ}-M$ scaling relations to derive the $Y_{SZ}-L_X$ scaling relation. The latter example is one where ignoring scatter corrections can result in biases as large as 20% – 30%.

Having derived the cluster scaling relations for each of the three data sets we consider, and having identified the origin of the differences them, we turn to investigate which of these analyses, if any, is consistent with cosmological expectations, for a WMAP7+BAO+ H_0 flat Λ CDM best fit cosmological model of Komatsu et al. (2011). Specifically, we consider each of the published L_X-M scaling relation in turn, convolve them with the Tinker et al. (2008) mass function appropriate for the aforementioned cosmology, and then compare the resulting predicted abundance with the X-ray luminosity function from the REXCESS catalog (Böhringer et al. 2002, 2004).

In addition to being interested in the X-ray and SZ scaling relations of galaxy clusters in their own right, one of our main motivations for pursuing this work is to take a closer look at the recent results by Planck Collaboration (2011c). In that work, it was found that the $Y_{SZ}-N_{200}$ scaling relation of optically-identified maxBCG clusters (Koester et al. 2007) were inconsistent with predictions derived from a combination of optical (Roza et al. 2009) and X-ray data sets (Arnaud et al. 2010). Because these predictions depend on the X-ray and SZ scaling relations of galaxy clusters, it is imperative that systematic uncertainties associated with these predictions be quantified, and that the scaling relations be self-consistently propagated in the presence of non-zero scatter. The results from this comparison will be presented in a subsequent paper, Roza et al. (in preparation), henceforth referred to simply as paper III. For the purposes of this work, this means we will focus our attention on cluster scaling relations at $z = 0.23$ exclusively, the median redshift of maxBCG clusters.

The layout of the paper is as follows. In § 2 we describe the data used in this work. This data takes the form of the L_X-M , $M-Y_X$, and $Y_{SZ}-Y_X$ scaling relations derived from each of the data sets we consider. Section 3 compares these three scaling relations to each other, and demonstrates that after correcting for the systematic offsets in X-ray observables identified in paper I — and tilting the M10 relations to an $f_{\text{gas}} \propto M^{0.15}$ model — all scaling relations are in good agreement with each other. We then turn to self-consistently deriving the

$Y_{SZ}-M$ (section 4) and $Y_{SZ}-L_X$ (section 5) scaling relations from the input scaling relations summarized in section 2. Section 5 also explicitly compares our self-consistently derived scaling relation with the data from Planck Collaboration (2011b). Section 6 tests whether the scaling relations from each of the three works are consistent with the observed cluster luminosity function in the current best-fit Λ CDM cosmology. Section 7 presents a summary of our results.

In all cases, scaling relation parameters are computed assuming a flat Λ CDM cosmology with $\Omega_m = 0.3$ and $h = 0.7$. When comparing abundances to cosmological expectations for a WMAP7+BAO+ H_0 cosmology, we use the best fit model from Komatsu et al. (2011) — which has $\Omega_m = 0.275$, $h = 0.702$, $n_s = 0.968$, and $\sigma_8 = 0.816$ — to compute the predicted halo mass function. As discussed in section 6, the scaling relations we use are still those that were computed assuming $\Omega_m = 0.3$. This is slightly inconsistent, but is necessary in the absence of precise knowledge of the degeneracies between each set of scaling relation parameters and cosmological parameters. We note, however, that because the changes in cosmological distances to low redshifts are very mild between the two cosmological models, we expect this inconsistency will only impact our predictions at the few percent level at most. This level of uncertainty is not enough to modify our conclusions.

Unless otherwise noted, all total masses, M , employ the M_{500} convention, where M_{500} is defined as the mass within a radius, R_{500} , that encompasses a mean interior density of 500 times the critical density of the universe, $\rho_c(z) = 3H^2(z)/8\pi G$.

2. DATA

We consider the cluster scaling relations as measured by three groups. The first is the P11-LS data set, which employs *Planck* and *XMM* data, and is comprised of Planck Collaboration (2011b), and the associated publications based on REXCESS clusters (Pratt et al. 2009; Arnaud et al. 2010). We note that in paper I we demonstrated that the $z \leq 0.13$ and $z \in [0.13, 0.3]$ galaxy clusters in Planck Collaboration (2011b) appear to be systematically difference. Consequently, and motivated by our ultimate goal of investigating the maxBCG $Y_{SZ}-N_{200}$ scaling relation, we will also be explicitly considering the subset of P11-LS galaxy clusters in the redshift range $z \in [0.13, 0.3]$, as appropriate for maxBCG systems. We refer to this subset of the P11-LS data set as P11-LS($z=0.23$). The second data set, V09, is comprised of Vikhlinin et al. (2009a) and Roza et al. (2012a), but relies on *Chandra* rather than *XMM* data. Finally, we consider the X-ray analysis of M10 (Mantz et al. 2010b), which is also *Chandra* based. Because this is the second in a series of papers, we will simply refer the reader to paper I for a more detailed description of each of the cluster data sets on which the scaling relations analysis is based. Here, we focus exclusively on the scaling relations reported in these works.

Table 1 summarizes the L_X-M , $M-Y_X$, and $Y_{SZ}-Y_X$ scaling relations as quoted in each of the above works, though modified when necessary to match the definitions for cluster observables adopted in this work (see below). We always adopt the pivot points reported by each individual work. The only exception to this rule is that in

TABLE 1
INPUT CLUSTER SCALING RELATIONS AT $z = 0.23$

Relation	χ_0	a	α	$\sigma_{\ln \psi \chi}$	Citation	Data Set
L_X-M_{500}	4.8	1.16 ± 0.09	1.61 ± 0.14	0.396 ± 0.039	Vikhlinin et al. (2009a)	V09
L_X-M_{500}	2.0	0.08 ± 0.08	1.62 ± 0.11	0.411 ± 0.070	Pratt et al. (2009)	P11-LS
L_X-M_{500}	10.0	2.11 ± 0.18	1.34 ± 0.05	0.414 ± 0.044	Mantz et al. (2010b)	M10
L_X-M_{500}	4.0	0.98	1.52	—	Reference	—
$M_{500}-Y_X$	3.0	1.53 ± 0.04	0.57 ± 0.03	$\leq 0.07^b$	Vikhlinin et al. (2009a)	V09
$M_{500}-Y_X$	2.0	1.23 ± 0.02	0.56 ± 0.02	$\leq 0.09^c$	Arnaud et al. (2010)	P11-LS
$M_{500}-Y_X$	10.0	2.25 ± 0.12	0.68 ± 0.04	0.072 ± 0.011	Mantz et al. (2010b)	M10
$M_{500}-Y_X$	4.0	1.65	0.6	—	Reference	—
$D_A^2 Y_{SZ}-CY_X$	8.0	1.877 ± 0.028	0.916 ± 0.035	0.082 ± 0.035	Rozo et al. (2012a)	V09
$D_A^2 Y_{SZ}-CY_X$	10.0	2.341 ± 0.038	0.828 ± 0.057	0.167 ± 0.039	Rozo et al. (2012a)	P11-LS($z=0.23$)
$D_A^2 Y_{SZ}-CY_X$	10.0	2.100 ± 0.09	1.0	$\leq 0.15^d$	This work	M10
$D_A^2 Y_{SZ}-CY_X$	10.0	2.303	1.0	—	Reference	—

^aIn all cases, we assume the ψ - χ relation takes the form $\langle \ln \psi \rangle = a + \alpha \ln(\chi/\chi_0)$. Our choice of units are $10^{14} M_\odot$ for mass, 10^{44} ergs/s for L_X , $10^{14} M_\odot \text{keV}$ for Y_X , and 10^{-5}Mpc^2 for $D_A^2 Y_{SZ}$ and CY_X . Unless otherwise noted, we set χ_0 to the reference scale in the cited work. All scaling relations are evaluated at $z = 0.23$, the median redshift of the maxBCG cluster sample.

^bVikhlinin et al. (2009a) only state that the scatter is undetectable given the errors on hydrostatic mass estimates, but that this is consistent with 7% scatter as predicted by Kravtsov et al. (2006). We implement this scatter in our analysis as a uniform prior in the variance with the maximum value quoted above.

^cArnaud et al. (2007) quote a scatter of 0.087, but provide no error bars. We implement this scatter in our analysis as a uniform prior on the variance using the maximum value quoted above.

^dUncertainty in the scatter is implemented as a uniform prior on the variance with the maximum value quoted above. The maximum value is chosen to be close to that derived from the Planck Collaboration (2011b) data by Rozo et al. (2012a).

the L_X - M relation from V09, where we set M_0 to the median mass of the Vikhlinin et al. (2009a) low redshift cluster sample, since the published relation used $1 M_\odot$ as its pivot point. We emphasize that in all cases, given two observables Y and X , our definition of the Y - X scaling relation is the expectation value $\langle \ln Y|X \rangle$. So, for instance, in the case of the L_X - M relation derived from X-ray samples, we only ever consider the Malmquist-bias corrected relations. This uniformity of definition is crucial for a self-consistent analysis of multi-variate cluster scaling relations. When considering stacked relations, we also take care to correct for the expected difference between $\ln \langle Y|X \rangle$ and $\langle \ln Y|X \rangle$ within the context of a log-normal scatter model.

Because our final goal (paper III) is to use the results from this work to investigate the discrepancy between theory and observations uncovered by Planck Collaboration (2011b), we have evaluated all scaling relations at $z = 0.23$, the median redshift of the maxBCG cluster sample. The Y_{SZ} - Y_X relation in Rozo et al. (2012a) is constrained only at $z \approx 0.1$, and we assume no redshift evolution when extending this result to $z = 0.23$, consistent with self-similar evolution. We note that all three works have different evolution terms in their scaling relations. For instance, for L_X - M , Pratt et al. (2009) assume $L_X \propto E(z)^{7/3}$, while Vikhlinin et al. (2009a) and Mantz et al. (2010b) find a best fit evolution $L_X \propto E(z)^{1.85 \pm 0.42}$ and $L_X \propto E(z)^{2.34 \pm 0.05}$ respectively. The self-similar expectation for soft-band X-ray luminosities is approximately $L_X \propto E(z)^2$. The evolution factors of P11-LS and M10 are nearly identical, with the evolution relative to V09 scaling as $E(z)^{0.49} \approx 1.06$. That is, the relative evolution from $z = 0$ to $z = 0.23$ can induce up to a 6% difference between the various works. This is also an extreme case, since all scaling relations have a redshift pivot point $z > 0$. Because these $\sim 5\%$ differences are typically much

smaller than that the differences between works, we will simply ignore them here, evaluating all scaling relations at $z = 0.23$ using each group's $E(z)$ evolution factors. Determining what the correct evolution factor is for each scaling relation is beyond the scope of this work.

We have also homogenized all data to common definitions: L_X is defined as the total X-ray luminosity within R_{500} in the $[0.1, 2.4]$ keV band, T_X is defined as the spectroscopic temperature in an annulus $R \in [0.15, 1]R_{500}$, M_{gas} is the total gas mass within R_{500} , $Y_X = M_{\text{gas}} \times T_X$, and Y_{SZ} is the integrated Compton parameter within a sphere of radius R_{500} . Whenever our definitions do not match the definitions employed in any of the works we consider, all data is rescaled as described in paper I. The data in Table 1 — in conjunction with the systematic offsets we estimated in paper I — form the basis of our analysis.

The different groups rely on different analysis techniques and different mass proxies when estimating cluster scaling relations. For the L_X - M analysis, V09 and P11-LS (via Pratt et al. 2009) rely on Y_X as a mass proxy, while Mantz relies on M_{gas} . In all cases, the mass-proxy (Y_X or M_{gas}) relation with mass is calibrated using hydrostatic mass estimates of relaxed galaxy clusters. V09 employs a likelihood fitting method that explicitly incorporates Malmquist bias, and tests their fitting routine using Monte Carlo cluster samples. The M10 analysis is very similar in spirit to the V09 analysis, but also explicitly incorporates the cosmological dependence of the cluster abundance function in the cluster scaling relations. Finally, Pratt et al. (2009) quote two different fits, corresponding to $BCES(Y|X)$ and $BCES$ -orthogonal fits. $BCES(Y|X)$ is closest to a likelihood fit in the absence of Malmquist bias. Since this fit is the one that is most comparable to those of V09 and M10, we only employ the $BCES(Y|X)$ Malmquist-bias corrected fit of Pratt et al. (2009) in this analysis. We caution that this

TABLE 2
MEAN LOG DIFFERENCES IN X-RAY PROPERTIES FOR SAMPLE PAIRS

Property	M10-V09	P11-LS-V09	P11-LS-M10 Low z	P11-LS-M10 High z	P05-V09
L_X^a	0.12 ± 0.02	-0.01 ± 0.02	-0.12 ± 0.02	-0.10 ± 0.03	—
M_{gas}^{ab}	0.03 ± 0.02	0.03 ± 0.02	-0.02 ± 0.03	-0.04 ± 0.02	—
T_X	—	-0.13 ± 0.02	—	-0.14 ± 0.05	—
Y_X^{ab}	—	-0.15 ± 0.03	—	-0.19 ± 0.05	—
M_{500}^{cd}	-0.03 ± 0.02	-0.12 ± 0.02	-0.05 ± 0.07	-0.37 ± 0.07	-0.18 ± 0.05
M_{500}^{de}	0.11 ± 0.11	-0.14 ± 0.03	-0.14 ± 0.03	-0.34 ± 0.06	—

^aOffset computed after outlier removal.

^bOffset computed after correction to a common aperture.

^cRelaxed/cool core only.

^dRelative to paper I, the offsets here are corrected by an 11% shift due to an update in *Chandra* calibration. This update was not applied to the masses quoted in the Tables in M10, but is applied for the scaling relations.

^eNon-relaxed/no cool core only.

is still not directly comparable to likelihood based approaches, since neglecting intrinsic scatter in the cost function being minimized gives clusters with small errors undue weight in the fit (see also Andreon & Hurn 2010).⁸ Importantly, as we show below, these differences in fitting methodology are not the primary drivers of the tension between the various scaling relation analyses.

Turning to the M - Y_X relation, Arnaud et al. (2010) rely on hydrostatic mass estimates of relaxed galaxy clusters to calibrate M - Y_X . Because Arnaud et al. (2010) did not quote the corresponding scatter, we rely instead on the value quoted in their previous work, Arnaud et al. (2007). Vikhlinin et al. (2009a) followed a similar approach to determine M - Y_X , but also fail to quote a constraint on the scatter, noting only that the data is consistent with no scatter, as well as with the predictions from Kravtsov et al. (2006). Thus, we place an upper limit on the scatter based on the value reported in Kravtsov et al. (2006). Mantz et al. (2010b) uses M_{gas} as a mass proxy, and the M - M_{gas} relation is itself calibrated based on hydrostatic mass estimates of relaxed galaxy clusters. We note too that Mantz et al. (2010b) report Y_X - M rather than M - Y_X . To obtain M - Y_X , we simply invert their relation. The corrections due to scatter are 2% in the amplitude (see equation A5), and are completely negligible both relative to their quoted uncertainty, and for the purposes of this work.

Finally, turning to the Y_{SZ} - Y_X scaling relation, we write this as

$$\langle \ln(D_A^2 Y_{\text{SZ}} | CY_X) \rangle = \alpha_{\text{SZ}} + \alpha_{\text{SZ}} \ln CY_X. \quad (1)$$

where D_A is the angular diameter distance, and C is a normalization constant,

$$C = \frac{\sigma_T}{m_e c^2} \frac{1}{\mu m_p} = 1.407 \times \frac{10^{-5} \text{ Mpc}^2}{10^{14} M_\odot \text{ keV}}, \quad (2)$$

where σ_T is the Thompson scattering cross section, m_e

⁸ We see very clear evidence of this, for instance, when measuring the Y_{SZ} - L_X relation from the $z \in [0.12, 0.3]$ clusters in Planck Collaboration (2011b): a $BCES(Y|X)$ fit results in steeper scaling relations than a likelihood fit because a few very massive clusters with extremely tight error bars dominate the penalty function being minimized. By including intrinsic scatter as a free parameter in the fit — as opposed to computing it a posteriori based on a fit including only statistical errors — these clusters are de-weighted, which flattens the resulting relations.

is the mass of the electron, m_p is the mass of a proton, and $\mu = 1.156$ is the mean molecular weight of the intra-cluster medium for solar abundance (variation in metallicities induces a $\approx 1\%$ uncertainty, completely negligible for our purposes).

Our constraints for the Y_{SZ} - Y_X scaling relation come from two sources. Roza et al. (2012a) constrain the Y_{SZ} - Y_X ratio using *Planck* and *Chandra* and this is the result we use later to estimate the Y_{SZ} - M relation in conjunction with the Vikhlinin et al. (2009a) data. Turning to the P11-LS data set, we noted in paper I that the P11-LS Y_{SZ}/Y_X ratio is different for $z \leq 0.13$ and $z \geq 0.13$ clusters, so rather than using the fit from Planck Collaboration (2011b) for the Y_{SZ} - Y_X relation, we have refit the P11-LS data for galaxy clusters in the $z \in [0.13, 0.3]$ redshift range using the method of Roza et al. (2012a). Our best fit scaling relation for the P11-LS($z=0.23$) data is included in Table 1.

It is important to emphasize that by choosing to use the Y_{SZ} - Y_X scaling relation derived from the P11-LS data in our predictions for the Y_{SZ} - M (and eventually N_{200} - M) scaling relations, we are diverging from the treatment of Planck Collaboration (2011c) for deriving the Y_{SZ} - N_{200} scaling relation. In that work, the Y_{SZ} - M relation used was that of Arnaud et al. (2010), which was derived from X-ray clusters alone. A more detailed discussion about the X-ray expectations for the Y_{SZ} - M scaling relation is presented in Roza et al. (2012a). Here, the point that we want to emphasize is that by working with the *observed* Y_{SZ} - Y_X scaling relation, we are explicitly testing whether all scaling relations are self-consistent, in the sense that a multivariate log-normal model can explain all observational data. Discussion of the consistency of the Y_{SZ} - Y_X scaling relation with X-ray expectations can be found in Roza et al. (2012a).

For completeness, we have also estimated the $D_A^2 Y_{\text{SZ}}/CY_X$ ratio that would be derived from a combination of the Planck Collaboration (2011b) data and the Mantz et al. (2010b) data (i.e. we are explicitly setting $\alpha_{\text{SZ}} = 1$ for the M10 data set). For all galaxy clusters shared by the M10 and P11-LS cluster samples, using the formalism from paper I we rescale the M_{gas} values in M10 to the R_{500} aperture adopted by P11-LS. We then directly compute Y_X for these systems, and use bootstrap resampling to compute the mean value of $\ln(D_A^2 Y_{\text{SZ}}/CY_X)$ at this aperture, along with the associ-

ated uncertainty. We find $\langle \ln(Y_{\text{SZ}}/Y_X) \rangle = -0.16 \pm 0.09$. We have confirmed that applying this exact method to the Vikhlinin et al. (2009a) data results in $\ln(Y_{\text{SZ}}/Y_X) = -0.20 \pm 0.04$, in perfect agreement with the more detailed analysis of Rozo et al. (2012a). We do not provide a scatter estimate since the errors in Mantz et al. (2010b) represent the expected uncertainty in Y_X , rather than just measurement errors. E.g. the error bar includes the expected scatter in gas clumping from cluster to cluster, which alone contributes $\approx 5\%$ scatter, already larger than the typical measurement error. The upper limit to the scatter quoted in Table 1 is *assumed* based on the scatter derived from the Planck Collaboration (2011b) data by Rozo et al. (2012a). Note, however, that comparison to the P11-LS and V09 values suggests the quoted upper limit is reasonable. The best fit $D_A^2 Y_{\text{SZ}}/CY_X$ is 0.82, corresponding to an amplitude parameter $a = 2.10$ for the $Y_{\text{SZ}}-Y_X$ relation.

For future reference, Table 2 shows the offsets in X-ray derived cluster observables from paper I. In fact, table 2 is a reproduction of Table 3 from paper I, albeit with some slight modifications. First, because the L_X-M relation of Pratt et al. (2009) relies on the mass calibration of Pointecouteau et al. (2005) — henceforth P05 — we have also explicitly added the mass offset between P05 and V09 for the purposes of our comparison (the offset was computed in paper I, but not included in Table 3 of that work). In addition, the scaling relations in Mantz et al. (2010b) were corrected for a *Chandra* calibration update, which uniformly shifts the masses of galaxy clusters by $\approx 11\%$. Because the cluster data tables in Mantz et al. (2010b) were *not* corrected for this calibration update, but the scaling relations were, we have corrected the observed P11-LS–M10 and M10–V09 offsets from paper I values to reflect the calibration employed by Mantz et al. (2010b) in their scaling relation analysis. This calibration update significantly improves the agreement between the P11-LS and M10 masses. Because Mantz quotes *ROSAT*-calibrated luminosities and M_{gas} , there is no corresponding shift in L_X or M_{gas} . While $M_{\text{gas}}(R_{500})$ does shift due to aperture effects, Table 2 quotes the M_{gas} offset at a fixed aperture, so an aperture correction is not necessary.

3. COMPARISON OF CLUSTER SCALING RELATIONS

Below, given a scaling relation $Y-X$, we will compare the 68% confidence regions in the $Y-X$ plane corresponding to the probability distribution $P(\ln Y | \ln X)$. These regions are estimated by performing 10^5 Monte Carlo draws of the amplitude and slope of each published scaling relation. We then evaluate $\langle \ln Y | \ln X \rangle$ along a logarithmically spaced grid in X , and compute the standard deviation of the resulting $\langle \ln Y | \ln X \rangle$ values at each point. This defines our estimate of the 68% confidence region of each cluster scaling relation in the $Y-X$ plane.

3.1. The L_X-M Relation

The top panel in Figure 1 compares the L_X-M_{500} relations derived from the P11-LS, V09, and M10 data sets. We remind the reader that the L_X-M relation we associate with the P11-LS data set is that of Pratt et al. (2009). The width of these bands reflects the quoted errors in each of the works being compared, as summarized in Table 1.

To more easily compare these relations, we compute the offset of each relative to a mean relation. The amplitude of the mean relation is defined as the average value of $\ln L_X$, evaluated at mass $M_{500} = 4 \times 10^{14} M_\odot$, as estimated from the P11-LS, V09, and M10 best fit scalings. The slope of the mean relation is likewise defined as the mean of the slopes of the three scaling relations. This mean scaling relation is only intended to be a reference to be subtracted from the three scaling relations: we do not ascribe any physical interpretation to it. More specifically, we do not advocate interpreting the mean scaling as more likely to be correct than any of its constituent elements.

The M10 errors of Table 1 are larger in amplitude than those quoted for the P11-LS and V09 data sets because they include systematic uncertainties, whereas the V09 and P11-LS errors are measurement errors only. The published M10 slope, however, has an error of only 0.05, compared with 0.11 and 0.14 for P11-LS and V09, respectively. These differences in the relative errors of the amplitude and slope explains why the P11-LS and V09 contours have an hourglass shape, while the M10 contours are nearly parallel lines.

The lower panel in Figure 1 shows the 68% confidence intervals of the L_X-M relations after subtracting the mean relation. We see that the P11-LS scaling relation is parallel to but clearly offset from the V09 scaling relation, while the M10 relation is flatter. We can test whether the difference in amplitude between these various scaling relations are due to differences in the raw X-ray cluster observables simply by shifting the amplitude of all the relations by the systematic offsets quoted in Table 2. If $\Delta \ln L_X = \langle \ln L_X \rangle_B - \langle \ln L_X \rangle_A$ is the mean offset between samples B and A in log-luminosity, and with $\Delta \ln M$ defined similarly for total mass, then the scaling relation from sample A can be observable-offset corrected to sample B by adding the constant $[\Delta \ln L_X - \alpha_A \Delta \ln M]$ to $\langle \ln L_X \rangle_A$. Assuming that the only difference between the two data sets A and B are the observable offsets characterized in paper I, applying these corrections to every data set should bring all scaling relations into good agreement with each other. For specificity, we observable-offset correct every scaling relation to the P11-LS scaling relation.

These amplitude shifts do not affect the slopes of the relations, and therefore cannot explain the tension between the slope derived by M10 and the remaining two data sets. Instead, the difference in slope can be traced to differences in $f_{\text{gas}}-M$ between the various works. Based on the results by Allen et al. (2008), Mantz et al. (2010b) assume that $f_{\text{gas}} = f_0$, a constant value. In paper I, we saw that given a different, power-law model, $f_{\text{gas}}(M) \sim M^\gamma$, the relation between the mass M of that model and that estimated by M10 is

$$M_{\text{M10}} = M \left(\frac{f_{\text{gas}}(M)}{f_0} \right)^{1.67} = M \left(\frac{M}{M_p} \right)^{1.67\gamma} \quad (3)$$

where M_p is the pivot mass of the $f_{\text{gas}}-M$ relation, and γ is the index of the $f_{\text{gas}}-M$ power-law. If ψ is a cluster observable where the M10 scaling relation is $\psi \propto M^{\alpha_{\text{M10}}}$, then the scaling relation the M10 scaling relation for an

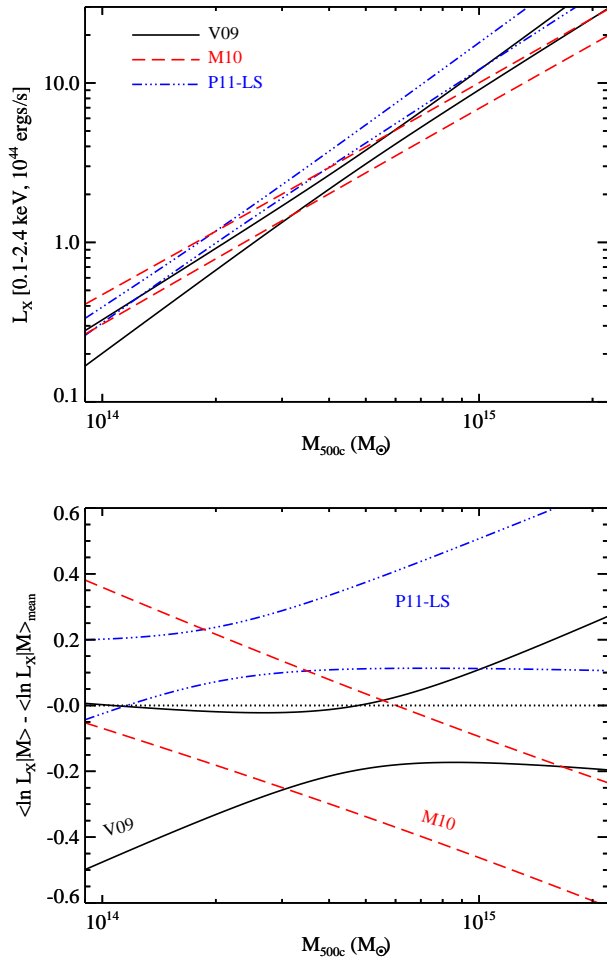


FIG. 1.— *Top panel*: 68% confidence band for the L_X – M relation for the P11-LS, V09, and M10, data sets, as labelled. All scaling relations are evaluated at the median redshift of the maxBCG sample, $z = 0.23$. *Bottom panel*: As per the top-panel, after subtracting out a reference mean scaling relation (see text for the definition of the mean scaling relation). Tensions are evident among the scaling relations.

$f_{\text{gas}} \propto M^\gamma$ would be

$$\psi = A \left[\left(\frac{M}{M_p} \right)^{1.67\gamma} \frac{M}{M_p} \right]^{\alpha_{M10}}. \quad (4)$$

Here, M_0 , A , and α_{M10} are the pivot point, amplitude, and slope of the ψ – M relation reported by Mantz et al. (2010b). The slope α relative to the mass M in this new f_{gas} model is

$$\alpha = \alpha_{M10}(1 + 1.67\gamma). \quad (5)$$

In the work of V09 and P11-LS, the slope γ of the f_{gas} – M relation is $\gamma \approx 0.1 - 0.2$. Setting $\gamma = 0.15$, and given $\alpha_{M10} = 1.34 \pm 0.05$, our model predicts an L_X – M slope $\alpha = 1.68 \pm 0.05$, resulting in an excellent match to the values of P11-LS and V09. Evidently, the reason that the M10 scaling relation appears flatter is that the f_{gas} model employed by M10 is not consistent with that of P11-LS or V09.

Figure 2 shows the difference in the L_X – M relation

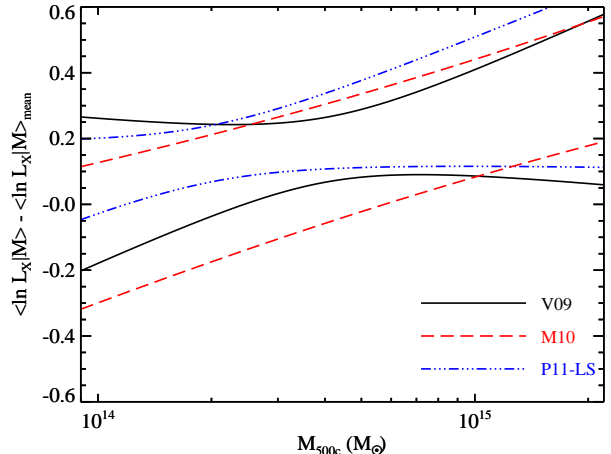


FIG. 2.— 68% confidence band for the L_X – M relation derived from the P11-LS, M10, and V09 data sets, as labelled. We have subtracted out a reference scaling relation as per the bottom panel of Figure 1. All scaling relations have been displaced along the L_X and M axis by the observable offsets relative to the P11-LS and P05 data sets characterized in Paper I. In addition, the M10 scaling relation has been tilted from a constant f_{gas} model to a model with $f_{\text{gas}} \propto M^{0.15}$. These corrections improve agreement among the scaling relations.

of V09, M10, and P11-LS, after accounting for the observable offsets in Table 2. The M10 relation is also tilted to an $f_{\text{gas}} \propto M^{0.15}$ model as described above.⁹ For M10, we show the L_X – M relation after shifting the M10 values using the P11-LS–M10 offset (dashed lines), and then also applying the offset between P11-LS and P05, which is necessary because the Pratt et al. (2009) scaling relation is calibrated based on P05. With these corrections, all scaling relations are in excellent agreement with each other. We conclude that the differences between the three works are driven by systematic offsets in X-ray observables, and the slope of the f_{gas} – M relation. In particular, the statistical treatment of each of the samples — i.e. the fact that each data set used a different statistical method for fitting the scaling relations and correcting for selection effects — appears to play a secondary role relative to the overall level of systematic offsets in the X-ray observables themselves.

3.2. The M – Y_X Relation

The top panel in Figure 3 shows the 68% confidence region for the M – Y_X relation of the three works considered here, after subtracting a mean scaling relation defined by a self-similar slope of $3/5$, and setting the amplitude to the mean amplitude of three works considered here at $Y_X = 4 \times 10^{14} M_\odot \text{keV}$. The parameters for this mean scaling relation are given in Table 1. The V09 and P11-LS relations are in excellent agreement, despite the large differences in the cluster-by-cluster comparison of mass and Y_X measurements, demonstrating that the systematic offsets from paper I move clusters along this best-fit relation. Unfortunately, because we do not know

⁹ We note that when applying a shift in the mass-axis and a tilt, it matters whether we shift first or tilt first. A uniform mass shift would only be appropriate for parallel relations, so we tilt first, then shift.

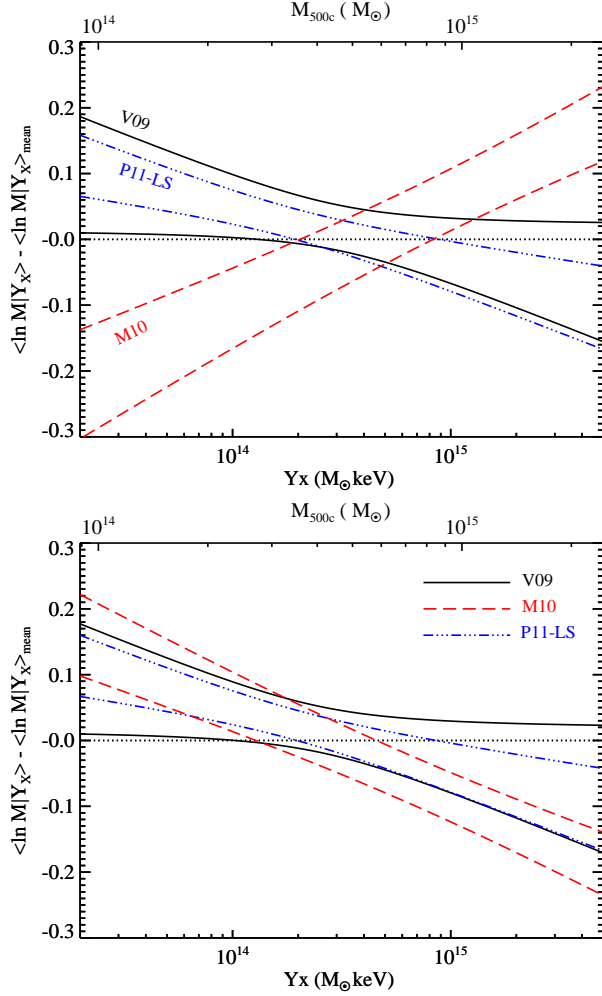


FIG. 3.— *Top panel*: 68% confidence band for the M - Y_X relation derived from the P11-LS, M10, and V09 data sets. For ease of comparison, we subtract out a reference mean relation as per the bottom panel in Figure 1. *Bottom panel*: As top panel, but after correcting for the systematic differences in cluster observables, and tilting the Mantz relation to that of an $f_{\text{gas}} \propto M^{0.15}$ model. As in the case of the L_X - M relation, all scaling relations are now in good agreement.

what is the source of the P11-LS-V09 offset in cluster observables, it is difficult to guess why this “conspiracy of errors” would happen. As for the M10 relation, we once again see a significantly different slope, so the amplitude offset depends on the mass scale under consideration.

The P11-LS-V09 comparison argues against instrumental calibration being the principal source of the observed systematic errors. Specifically, a temperature bias, b_T , induces a bias $b_M = b_T^{1.5}$ in hydrostatic masses (Vikhlinin et al. 2006). This in turn induces a bias $b_{\text{gas}} = b_M^{0.4} = b_T^{0.6}$ via aperture effects, so the net bias in Y_X is $b_Y = b_T^{1.6}$. Letting $\alpha \approx 5/3$ be the slope of the Y_X - M relation, we see that a temperature calibration bias b_T will induce a bias $b_T^{1.5\alpha-1.6} \approx b_T^{0.9}$ in the amplitude of the Y_X - M relation. In other words, an overall temperature bias due to instrumental calibration does not appear to shift galaxy clusters along the scaling relation.

The lower panel in Figure 3 illustrates the offset-corrected scaling relations. We have also tilted the M10

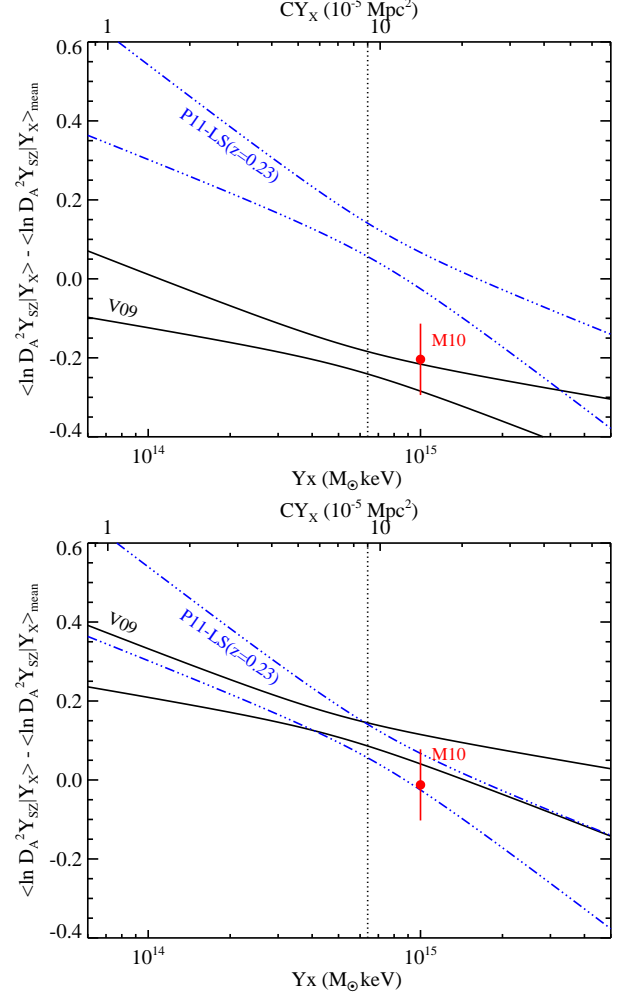


FIG. 4.— *Top panel*: The $Y_{\text{SZ}}-Y_X$ relation at $z = 0.23$ for each of the data sets we consider, as labelled. There are large differences between each of the data sets. *Bottom panel*: The $Y_{\text{SZ}}-Y_X$ relation after correcting for cluster observable systematic offsets, and correcting the Vikhlinin curve for the expected redshift evolution. The vertical dotted line is the pivot point of the V09 relation.

relation to that of a $\gamma = 0.15$ f_{gas} model. As in the case of L_X - M , after these corrections all three scaling relations are in agreement within the expected errors.

3.3. The $Y_{\text{SZ}}-Y_X$ Scaling Relation

The top panel in Figure 4 shows the $Y_{\text{SZ}}-Y_X$ scaling relation after subtracting out the reference relation $\langle \ln D_A^2 Y_{\text{SZ}} | Y_X \rangle = \ln(CY_X)$ where C is given by equation 2, and assuming both $D_A^2 Y_{\text{SZ}}$ and CY_X are measured in the same units. Because we assume $\alpha = 1$ for the Mantz data, we only place a single point with error bars at the pivot point of the sample. There are large differences between the P11-LS($z=0.23$) and the V09 and M10 samples.

The bottom panel in Figure 4 corrects the V09 and M10 scaling relations for the observable offsets from Table 2 relative to the P11-LS($z=0.23$) data. The V09 scaling relation is modified using the shifts relative to the low-redshift P11-LS data, and then again by the redshift correction between low and high redshift based on the Y_{SZ}/Y_X ratio. The M10 value is shifted using the

Y_X shift relative to P11-LS($z=0.23$) directly. With these corrections, all data sets agree on the amplitude of the Y_{SZ}/Y_X relation, though some differences in the slope are apparent.

3.4. Summary of Results

The main result of this section is very clear: despite differences in fitting methods as well as differences in the treatment of selection effects, after accounting for the systematic differences in derived X-ray cluster observables and modeling of the slope of the $M_{gas}-M$ relation, all scaling relations are in good agreement with each other. In other words, systematics in the treatment of selection effects and/or fitting methods are clearly subdominant to the overall systematic offset in the input data used to derive the scaling relations.

4. THE $Y_{SZ}-M$ RELATION AS CALIBRATED FROM X-RAYS

Having specified the $M-Y_X$ and $Y_{SZ}-Y_X$ relation, the $Y_{SZ}-M$ relation is nearly completely specified. We now derive expressions for the amplitude and slope of the $Y_{SZ}-M$ scaling relation in terms of the others, which we then apply to each of the X-ray data sets considered in this work.

Part of the motivation for this work is simply to transport the $M-Y_X$ calibration from X-ray data sets to $Y_{SZ}-M$, in order to enable cosmological interpretations of SZ cluster samples. Just as importantly, however, we wish to determine the differences in the predicted $Y_{SZ}-M$ scaling relation for each of these data sets, as these differences will necessarily have an important impact in the interpretation of the SZ–richness scaling relations of maxBCG galaxy clusters (paper III).

4.1. Method

We define

$$y_x = \ln(Y_X/Y_0) \quad (6)$$

$$y_{sz} = \ln(D_A^2 Y_{SZ}/\Delta_0^2) \quad (7)$$

$$m = \ln(M/M_0) \quad (8)$$

$$(9)$$

where the normalization constants Y_0 , Δ_0^2 , and M_0 are chosen so as to decorrelate the amplitude and slope of the cluster scaling relations. In the previous section, we specified the $Y_{SZ}-Y_X$ and $M-Y_X$ scaling relation. Combining this two relations, we can arrive at an expression for the $Y_{SZ}-M$ scaling relation. Specifically, let us write

$$\langle y_{sz}|m \rangle = a_{sz|m} + \alpha_{sz|m} m \quad (10)$$

$$\langle m|y_x \rangle = a_{m|x} + \alpha_{m|x} y_x \quad (11)$$

$$\langle y_{sz}|y_x \rangle = a_{sz|x} + \alpha_{sz|x} y_x \quad (12)$$

We wish to solve for $a_{sz|m}$ and $\alpha_{sz|m}$ in terms of known parameters. Using a local power-law model for cluster abundances — see Appendix A, and specifically equations A5 and A12 (see also White et al. 2010) — one has that the parameters of the various relations above are related via

$$a_{sz|x} = [a_{sz|m} + \alpha_{sz|m} a_{m|x}] + r_{sz,x|m} \beta \alpha_{sz|m} \sigma_{m|x} \sigma_{m|sz} \quad (13)$$

$$\alpha_{sz|x} = \alpha_{sz|m} \alpha_{m|x} \quad (14)$$

where $r_{sz,x|m}$ is the correlation coefficient between y_{sz} and y_x at fixed m , β is the slope of the halo mass function ($dn/d\ln M \propto M^{-\beta}$), and $\sigma_{m|x}$ and $\sigma_{m|sz}$ are the scatter in m at fixed y_x and y_{sz} respectively. Note the term in square brackets in equation 13 is simply the naive relation obtained from plugging equation 11 into equation 10.

Since both $\alpha_{m|x}$ and $\alpha_{sz|x}$ are known from the previous section, we can readily solve for $\alpha_{sz|m}$,

$$\alpha_{sz|m} = \frac{\alpha_{sz|x}}{\alpha_{m|x}}. \quad (15)$$

To solve for $a_{sz|m}$ from equation 13, we must first be able to estimate the correction term depending on the correlation coefficient, which requires that we know both r and $\sigma_{m|sz}$. While equation A13 in Appendix A relates these two quantities, one still needs an additional independent input to close the system.

We arrive at an additional relation between r and $\sigma_{m|sz}$ using a simple model for how Y_{SZ} and Y_X are correlated. Motivated by the fact that Roza et al. (2012a) find that the intrinsic scatter in the $Y_{SZ}-Y_X$ relation is consistent with zero, we make the assumption that the noise in y_{sz} has two contributions: an intrinsic contribution δy_{int} , which is identical and perfectly correlated with the intrinsic noise in y_x , reflecting variations in the details of the physical properties of the intra-cluster medium, and an additional noise δy_{lss} that is due to structures along the line of sight to the clusters, and which is uncorrelated with fluctuations in y_x . Setting $\langle \delta y_{int}^2 \rangle = \sigma_{x|m}^2$, $\langle \delta y_{int} \delta y_{lss} \rangle = 0$, $\delta y_{sz} = \delta y_{int} + \delta y_{lss}$, and $\delta y_x = \delta y_{int}$, we find

$$r_{sz,x|m} = \frac{\langle \delta y_{sz} \delta y_x \rangle}{\sigma_{x|m} \sigma_{sz|m}} = \frac{\sigma_{x|m}}{\sigma_{sz|m}}. \quad (16)$$

In addition, from equation A6 in Appendix A, we have

$$\sigma_{m|x} = \alpha_{m|x} \sigma_{x|m}, \quad (17)$$

with a similar relation for y_{sz} . Putting these two together, we can rewrite equation 13 as

$$a_{sz|m} = [a_{sz|x} - \alpha_{sz|m} a_{m|x}] - \frac{\beta}{\alpha_{m|x}} \sigma_{m|x}^2. \quad (18)$$

As a rough order of magnitude, we expect a slope of the halo mass function $\beta \approx 3$, and $\alpha_{m|x} \approx 3/5$, which for 10% scatter in mass corresponds to a nearly negligible 5% amplitude shift. Together, equations 18 and 15 completely specify the $Y_{SZ}-M$ scaling relation in terms of known parameters (i.e. in terms of the $Y_{SZ}-Y_X$ and $M-Y_X$ scaling relation parameters).

Let us now turn to the scatter in the $Y_{SZ}-M$ scaling relation. From equation A13 in Appendix A we have

$$\sigma_{sz|x}^2 = \alpha_{sz|m}^2 [\sigma_{m|x}^2 + \sigma_{m|sz}^2 - 2r_{sz,x|m} \sigma_{m|x} \sigma_{m|sz}]. \quad (19)$$

Using equations 16 and A6, we can rewrite the r term above in terms of $\sigma_{m|x}$ only. Solving for $\sigma_{m|sz}^2$, and using equation A6 again to obtain $\sigma_{sz|m}$ from $\sigma_{m|sz}$ we arrive at

$$\sigma_{sz|m}^2 = \sigma_{sz|x}^2 - \sigma_{m|x}^2 \frac{\alpha_{sz|x} (\alpha_{sz|x} - 2)}{\alpha_{m|x}^2}. \quad (20)$$

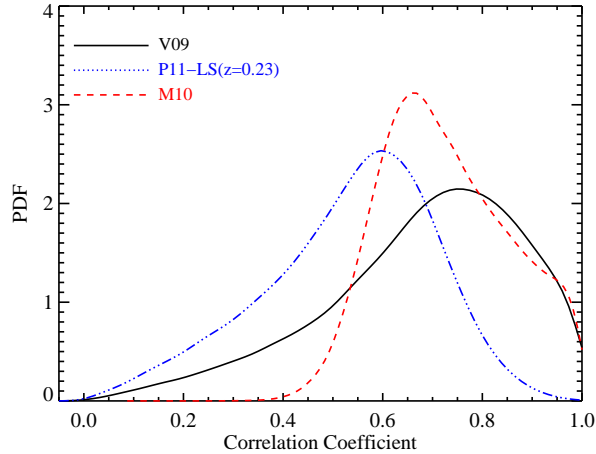


FIG. 5.— Likelihood distribution for the correlation coefficient $r \equiv \text{Cov}(y_{sz}, y_x) / \sigma_{x|m} \sigma_{sz|m}$ for each of the three data sets we consider, as labelled. The maximum likelihood value for r , as well as the upper and lower limits defining the 68% confidence contour, are summarized in Table 3.

This gives $\sigma_{sz|m}$ in terms of known quantities. To solve for $r_{sz,x|m}$, we again use equations 16 and A6 to write $\sigma_{sz|m}$ in terms of $r_{sz,x|m}$ and $\sigma_{m|x}$, and solve for $r_{sz,x|m}$. We arrive at

$$r_{sz,x|m} = \left[\alpha_{m|x}^2 \frac{\sigma_{sz|x}^2}{\sigma_{m|x}^2} + \alpha_{sz|x} (2 - \alpha_{sz|x}) \right]^{-1/2}. \quad (21)$$

We evaluate the right hand side of the above equation using the central values from the V09 data set to arrive at $r_{sz,x|m} = 0.84$. As expected, the fluctuations about the mean in Y_{SZ} and Y_X at fixed mass are heavily correlated. The likelihood for the correlation coefficient r is shown in Figure 5, and the corresponding constraint is summarized in Table 3.

Having derived analytical relations between the input $M-Y_X$ and $Y_{SZ}-Y_X$ scaling relation parameters, and the $Y_{SZ}-M$ scaling relation parameters, we now wish to propagate the uncertainty in these input scaling relations (see Table 1) into uncertainty in the $Y_{SZ}-M$ relation. The first step is to specify the choice of units for each data set. The mass units M_0 are set to $M_0/10^{14} M_\odot = 4.8, 5.5,$ and 10.0 for the V09, P11-LS, and M10 data sets. The slope of the halo mass function β is evaluated at this pivot point for our fiducial cosmology, and the corresponding values are tabulated in Table 3. For the SZ units, we set $\Delta_0^2 = 10^{-5} \text{ Mpc}^2$. We adopt the pivot point Y_0 quoted for the $M-Y_X$ relation. Our choice of units for M_0 is set so as to match the pivot point in the L_X-M relation, unless doing so induces strong covariance between the amplitude and slope of the $Y_{SZ}-M$ scaling relation. This only occurs for the P11-LS($z=0.23$) data set, where the mass pivot of the Planck Collaboration (2011b) and Arnaud et al. (2010) data are not well matched. In this case, we chose our mass units to decorrelate the amplitude and slope of the $Y_{SZ}-M$ scaling relation, since this is the quantity of interest in this section.

To determine the uncertainty in the $Y_{SZ}-M$ scaling relation, we randomly generate the $M-Y_X$ and $Y_{SZ}-Y_X$ scaling relation parameters from the values quoted in Ta-

ble 1. These randomly drawn parameters are input into equations (15), (18) and (20) to solve for the $Y_{SZ}-M$ scaling relation parameters. Table 1 only quotes uncertainties for the scatter $\sigma_{m|z}$ for the M10 data set. For the Vikhlinin et al. (2009a) and Arnaud et al. (2010) $M-Y_X$ relation, we adopt a uniform prior on the variance $\sigma_{m|x}^2$ with $\sigma_{m|x}^2 \leq 0.07^2$ and $\sigma_{m|x}^2 \leq 0.09^2$ respectively. As for the M10 $Y_{SZ}-Y_X$ scaling relation, we assume a conservative flat prior on the variance $\sigma_{sz|x}^2 \leq 0.15^2$. We perform 10^5 independent random draws to estimate the resulting likelihood distributions, also enforcing the prior $|r| \leq 1$. The resulting $Y_{SZ}-M$ scaling relations are summarized in Table 3 and Figure 6, and the likelihood distributions are shown in Figure 10. We emphasize that because the mass pivots are different for different relations, one cannot use Figure 10 to determine whether the various $Y_{SZ}-M$ relations are consistent with one another. For that purpose, one should focus instead on Figure 6.

Finally, a warning. The relations between the amplitudes, slopes, and scatters of the various relations denoted above are exactly correct. However, our Monte Carlo method for propagating the uncertainties in the $Y_{SZ}-Y_X$ and $M-Y_X$ scaling relations into the $Y_{SZ}-M$ scaling relation explicitly assumes that the uncertainties of these input scaling relations are uncorrelated. However, in all cases many of the same clusters were used as inputs in the analysis leading to the input scaling relations were shared. So, for instance, some of the clusters that contribute to the $Y_{SZ}-Y_X$ calibration also contribute to the $M-Y_X$ calibration. In this case, the most correct analysis would be to do a multi-variate scaling relation analysis fit from the start, something which is not really feasible given the available data, and certainly beyond the scope of this work. With this caveat in mind, we proceed.

4.2. Results

Figure 6 shows the 68% confidence contours of the $Y_{SZ}-M$ scaling relations corresponding to each of the three sets of parameters summarized in Table 3. As usual, we subtract out a reference scaling relation, defined by a self-similar slope of 5/3. The amplitude of the reference scaling relation is defined by the mean amplitude at $M = 5 \times 10^{14} M_\odot$ between the V09, M10, and P11-LS($z=0.23$) data sets, and is summarized in Table 3. There is a clear amplitude offset between the V09 and P11-LS($z=0.23$) data which mirrors the difference in the L_X-M relation. The offset is partly caused by the systematic differences in mass calibration between P11-LS and V09, and partly by the redshift evolution in Y_X between low and high redshifts in the P11-LS data. The M10 relation is in good agreement with the V09 relation where the samples overlap ($M \sim 10^{15} M_\odot$), but the slope of the relation is very different, reflecting the differences in slope of the f_{gas} model.

Comparing our self-consistently propagated scaling relation for the P11-LS($z=0.23$) data set to that published in P11-LS, we see that ours has a higher amplitude, and a different slope. There are various reasons for this. First, an amplitude offset is expected given the difference in the Y_{SZ}/Y_X ratio between low and high redshift cluster samples discussed in paper I. Likewise, a difference in the slope of the $Y_{SZ}-Y_X$ relation should also result in different

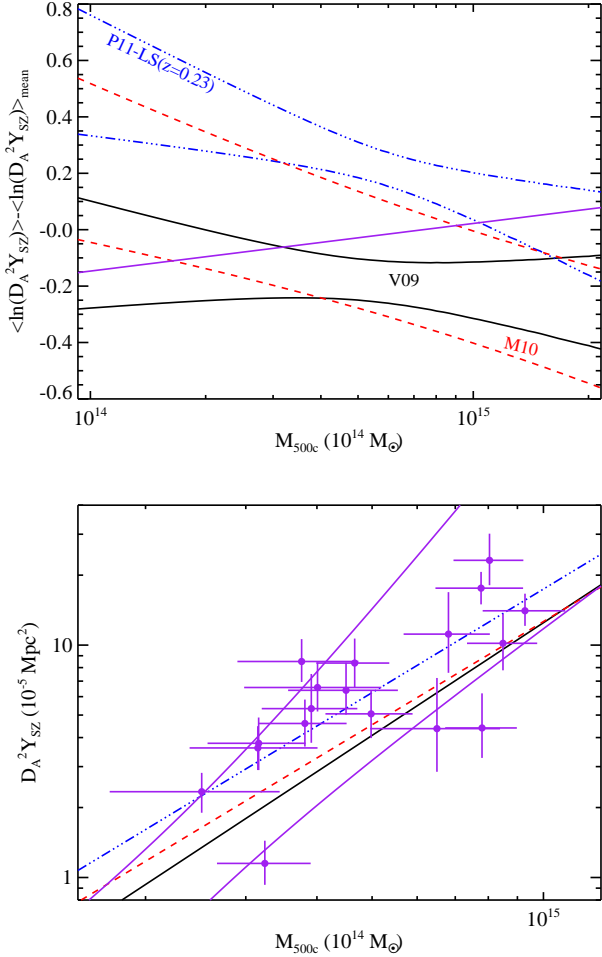


FIG. 6.— *Top panel*: 68% confidence regions for the $Y_{\text{SZ}}-M$ scaling relation as determined by each of the four data sets we consider, as labeled. The purple line is the $Y_{\text{SZ}}-M$ scaling relation at $z = 0.23$ as quoted in Planck Collaboration (2011b). *Bottom panel*: Comparison of our derived scaling relations with the data from Marrone et al. (2011). The purple lines show the 68% confidence regions of the $M-Y_{\text{SZ}}$ scaling relation from that work. Otherwise, the color key is the same as for the top panel: red=M10, blue=P11-LS($z=0.23$), black=V09.

$Y_{\text{SZ}}-M$ slopes. The role of selection effects is a bit more unclear: P11-LS correct for selection effects by performing Monte Carlo samples, which leads to a lowering of the amplitude by 7%. On the other hand, we estimated scatter corrections to the naive plug-in method — which we expect is roughly equivalent to directly fitting $Y_{\text{SZ}}-M$ by setting all clusters to the mass $M(Y_X)$ — to lead to a 5% downwards correction, with some uncertainty associated with the value of the scatter. Because we expect that the Monte Carlo procedure of P11-LS would detect the scatter corrections introduced in this work, it is not surprising that the two corrections are nearly identical, and it suggests that selection function effects that are over and beyond these scatter corrections are negligible, as would be expected for scaling relations with tight scatter.

In an attempt to shed further light on the $Y_{\text{SZ}}-M$ scaling, the bottom panel of Figure 6 compares our predicted scaling relations to the LoCuSS sample measurements of

Marrone et al. (2011). That work estimated M_{500} using weak lensing shear measurements (Okabe et al. 2010). The individual data points are shown, while the solid purple lines span the 68% confidence region of the corresponding $Y_{\text{SZ}}-M$ relation. Because the intrinsic scatter is small, the corrections from this inversion are completely negligible relative to the statistical errors. Consequently, we ignored the scatter corrections when estimating the $Y_{\text{SZ}}-M$ relation parameters from the published $M-Y_{\text{SZ}}$ relation parameters.¹⁰ It is clear from the figure that their best fit scaling relation is in agreement with all three of the scaling relations we computed, so the LoCuSS data is not yet of high enough quality to unambiguously prefer one data set over another.

In this context, we note that a recent paper by Planck Collaboration (2012) has noted there are large systematic differences between their X-ray masses and the weak lensing masses of Okabe et al. (2010). We treat this problem in more detail in paper III. Here, it suffices to note that these systematic differences are not sufficient to create statistical tension between our results and those of Marrone et al. (2011) because of the large uncertainties in the latter work.

5. THE $Y_{\text{SZ}}-L_X$ RELATION

We now use the $Y_{\text{SZ}}-M$ and L_X-M scaling relations to self-consistently derive the $Y_{\text{SZ}}-L_X$ scaling relation. There are two motivations for this work. First, in the absence of systematic errors, our prediction for the $Y_{\text{SZ}}-L_X$ scaling relation must be fully self-consistent with the observed $Y_{\text{SZ}}-L_X$ relation. We have seen, however, that the scaling relations of galaxy clusters systematically vary from data set to data set. If we can determine that for a given data set our predicted $Y_{\text{SZ}}-L_X$ relation is not consistent with the observed $Y_{\text{SZ}}-L_X$ relation, then that is strong evidence that these exist systematic errors in the corresponding data set.

To the extent that a multivariate Gaussian approximation is a valid description of the scatter about mean scalings, any data set whose relations are not self-consistent (i.e., deviate from the expectations of Appendix A) necessarily suffers from systematic uncertainties. By the same token, the $Y_{\text{SZ}}-L_X$ scaling relation plays a critical self-consistency constraint for the SZ-optical scaling relations of galaxy clusters, and will therefore provide an important test of the interpretation of the Planck Collaboration (2011c) results presented in paper III.

5.1. Method

Similar to the previous section, we define

$$l_X = \ln(L_X/L_0). \quad (22)$$

Having already specified the $Y_{\text{SZ}}-M$ and the L_X-M scaling relations, the $Y_{\text{SZ}}-L_X$ relation is constrained, up to the value of the covariance between Y_{SZ} and L_X at fixed M . Because the scatter in L_X is dominated by the

¹⁰ We did, however, implement a prior that the slope of the $M-Y_{\text{SZ}}$ relation must be larger than $\alpha_{m|sz} \geq 0.2$. Because the amplitude of the $Y_{\text{SZ}}-M$ relation is $-a_{m|sz}/\alpha_{m|sz}$ (see equation A5), allowing $\alpha_{m|sz}$ to get close to zero is both unphysical and numerically unsound.

TABLE 3
DERIVED CLUSTER SCALING RELATIONS AT $z = 0.23$

Relation	χ_0	β	$\ln \psi_0$	α	$\sigma_{\ln \psi \chi}$	r	Sample
$D_A^2 Y_{\text{SZ}}-M$	4.8	2.75	1.34 ± 0.07	1.61 ± 0.11	0.12 ± 0.03	$0.75^{+0.20}_{-0.20}$	V09
$D_A^2 Y_{\text{SZ}}-M$	5.5	2.93	1.97 ± 0.06	1.48 ± 0.12	0.20 ± 0.04	$0.60^{+0.15}_{-0.20}$	P11-LS($z=0.23$)
$D_A^2 Y_{\text{SZ}}-M$	10.0	3.95	2.54 ± 0.20	1.48 ± 0.09	0.15 ± 0.03	$0.66^{+0.18}_{-0.09}$	M10
$D_A^2 Y_{\text{SZ}}-M$	5.0	—	1.58	5/3	—	—	Reference
$D_A^2 Y_{\text{SZ}}-L_X$	4.0	—	1.33 ± 0.13	1.01 ± 0.11	0.35 ± 0.07	—	V09
$D_A^2 Y_{\text{SZ}}-L_X$	4.0	—	1.45 ± 0.15	0.92 ± 0.10	0.32 ± 0.10	—	P11-LS($z=0.23$)
$D_A^2 Y_{\text{SZ}}-L_X$	10.0	—	2.27 ± 0.31	1.10 ± 0.08	0.40 ± 0.08	—	M10

^a In all cases, we assume the ψ - χ relation takes the form $\ln \psi = \ln \psi_0 + \alpha \ln(\chi/\chi_0)$. Our choice of units are $10^{14} M_\odot$ for mass, 10^{44} ergs/s for L_X , and 10^{-5} Mpc² for $D_A^2 Y_{\text{SZ}}$. All scaling relations are appropriate for $z = 0.23$, the median redshift of the maxBCG cluster sample. The quantity β is the slope of the halo mass function at the pivot scale of the $Y_{\text{SZ}}-M$ relation. All errors are the standard deviation of the distribution, except for the correlation coefficient r between Y_{SZ} and Y_X at fixed mass. The likelihood distribution for r is highly non-gaussian (see Figure 5), so we quote the maximum likelihood value, and the error bars define the 68% likelihood contour.

details of the X-ray emission from the core of galaxy clusters, while the scatter in Y_{SZ} is dominated by projection effects, the two are not likely to be correlated at any significant level, so one might expect $r_{sz,l|m} \approx 0$. On the other hand, Stanek et al. (2010) derived theoretical predictions for the correlation coefficient between Y_{SZ} and L_{bol} , the bolometric X-ray luminosity, based on numerical simulations. They find $r \approx 0.8$, which reflect the fact that clusters with more gas and/or hotter gas will have both higher X-ray luminosity and higher pressure. In the absence of more detailed information, we adopt a uniform prior $r_{sz,l|m} \in [0, 1]$.

Using the formulae in Appendix A (see also White et al. 2010), and following arguments similar to those in the previous section, we can write the amplitude, slope, and scatter, of the $Y_{\text{SZ}}-L_X$ scaling relation in terms of the parameters characterizing the $Y_{\text{SZ}}-M$ and the L_X-M scaling relation. In the notation of the previous section, we find

$$a_{sz|l} = \left[a_{sz|m} - \frac{\alpha_{sz|m}}{\alpha_{l|m}} a_{l|m} \right] + \beta \alpha_{sz|m} \sigma_{m|l} [r_{sz,l|m} \sigma_{m|sz} - \sigma_{m|l}] \quad (23)$$

$$\alpha_{sz|l} = \frac{\alpha_{sz|m}}{\alpha_{l|m}} \quad (24)$$

$$\sigma_{sz|l}^2 = \alpha_{sz|m}^2 \left[\sigma_{m|l}^2 + \sigma_{m|sz}^2 - 2r_{sz,l|m} \sigma_{m|l} \sigma_{m|sz} \right] \quad (25)$$

The term in square brackets is the naive relation one would obtain in the absence of scatter, and the scatter in mass at fixed observable is related to the scatter in observable at fixed mass via equation A6. To get an order of magnitude estimate for the correction term, we set $\beta = 3$, $\alpha_{sz|m} = 5/3$, $r_{sz,l|m} = 0$, and $\sigma_{m|l} = 0.25$, which yields a correction term ≈ -0.3 , corresponding to a 30% offset in Y_{SZ} at fixed L_X , a very significant correction. If we set $r_{sz,l|m} = 1$ instead, and adopt $\sigma_{m|sz} = 0.1$, the correction is only reduced to ≈ -0.2 , still large.

To apply this formalism, we must again specify units. We adopt as mass units the pivot point of the $Y_{\text{SZ}}-M$ relation, which matches that of the L_X-M relation for the V09 and M10 data sets. For the P11-LS data set, the pivot point of the L_X-M relation is lower than that of

the $Y_{\text{SZ}}-M$ relation. When sampling the L_X-M scaling relation, we randomly draw the amplitude and slope at the pivot point of the L_X-M relation, and then shift the amplitude to the new pivot point. This procedure explicitly includes the induced covariance between amplitude and slope at the new pivot point. The scaling relations are sampled 10^4 times, and the corresponding $Y_{\text{SZ}}-L_X$ parameters constrained from the Monte Carlo distribution. The units for L_X are chosen so as to decorrelate the amplitude and slope of the $Y_{\text{SZ}}-L_X$ relation, and are set to $L_0 = 3 \times 10^{44}$ ergs/s for the V09 and P11-LS data sets, and $L_X = 10^{45}$ ergs/s for the M10 data set. The units for $D_A^2 Y_{\text{SZ}}$ are set to $\Delta_0^2 = 10^{-5}$ Mpc² in all cases. As in the case of the $Y_{\text{SZ}}-M$ relation, we note that in principle the uncertainties in the input scaling relation parameters can be correlated, for instance due to shared clusters in the calibration of the L_X-M and $Y_{\text{SZ}}-M$ scaling relations, so the same caveat mentioned in the previous section holds for this discussion as well.

5.2. Results

Figure 11 shows the likelihood for each of the data sets we consider. There are significant differences in amplitude between the various works, but the uncertainties are also large. We compare each of our predictions to the Planck Collaboration (2011b) data. Figure 7 shows all galaxy clusters in Planck Collaboration (2011b) in the redshift slice $[0.13, 0.3]$. We adopt this cut to ensure that we only look at clusters near the redshift of interest ($z = 0.23$), and also because from paper I we know that the low and high redshift populations of the Planck Collaboration (2011b) clusters appear to have different properties. Note that because Y_{SZ} depends on R_{500} , when comparing our predictions to the P11-LS Y_{SZ} data we need to account for the systematic difference in mass between the various groups as per the Appendix B in paper I. We do so by shifting the data points rather than our predictions, though we also note that because Y_{SZ} depends only mildly on R_{500} , the shifts due to aperture corrections are much smaller than the differences between the predicted scaling relations (i.e. aperture corrections in Y_{SZ} are a second order effect).

In addition to showing the data points themselves, Figure 7 shows as a dark-green line our best-fit relation to

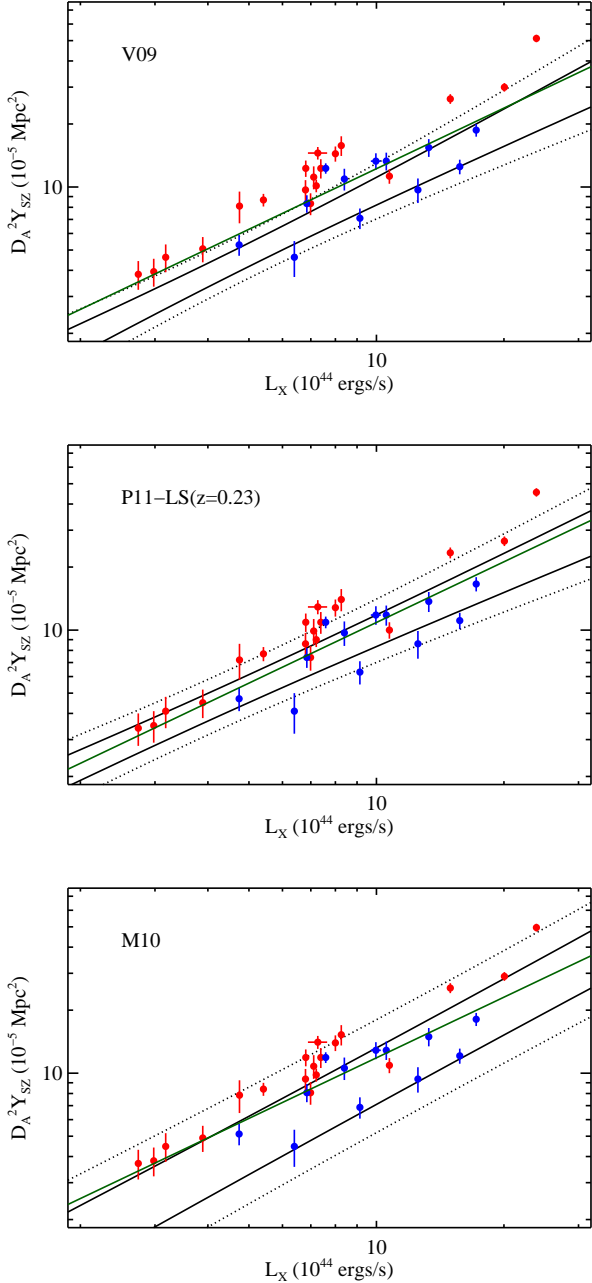


FIG. 7.— Comparison between the Planck Collaboration (2011b) data for clusters in the redshift range $z \in [0.12, 0.3]$ and the $Y_{\text{SZ}}-L_X$ relations derived self-consistently from the $Y_{\text{SZ}}-M$ and L_X-M relations. The green line is our best fit to the Planck Collaboration (2011b) data, while the black solid (dotted) lines mark the 1σ (2σ) confidence regions of the mean scaling relation. Blue points are cool-core systems, while red points are not.

the P11-LS($z=0.23$) data. The amplitude of the fit is corrected for selection effects based on the results of P11-LS, which amount to a 9% reduction of the best fit amplitude. The 1σ and 2σ regions for each of the three predicted scaling relations are shown in Figure 7 as black solid and dotted lines respectively. The best fit relation to the data is clearly that derived from the P11-LS($z=0.23$) scaling relations, but the best fit relation is within the 2σ regions of the predicted scaling relations for all three data sets.

Consequently, we are unable to identify which data sets suffer from systematic errors using the $Y_{\text{SZ}}-L_X$ measurements from Planck Collaboration (2011b).

We have also attempted to compare our self-consistently propagated scaling relations to the data from Planck Collaboration (2011a), henceforth referred to as P11-X. P11-X assembled a heterogeneous X-ray cluster catalog, the MCXC catalog (Piffaretti et al. 2011), and used it to measure the $Y_{\text{SZ}}-L_X$ relation. Unfortunately, this comparison is not trivial. As noted in that work, the $Y_{\text{SZ}}-L_X$ scaling relation from the MCXC sample and the P11-LS scaling relations are not consistent, with the MCXC relation shifted towards more luminous systems (lower amplitude). This is illustrated in Figure 8, which shows the 2σ regions of the P11-X results as the solid purple lines.¹¹ Also shown as purple squares with errors are the binned data from the same work. The dashed dark-green lines are the 2σ confidence regions as reported in Table 2 of Planck Collaboration (2011b, i.e. the P11-LS result). The $z \in [0.12, 0.3]$ clusters in P11-LS are shown as circles with error bars, and our own fit to the data is similar to that of P11-LS. We see that the 2σ boundaries of the two relations — that of P11-LS and that of Planck Collaboration (2011a) — barely overlap. The amplitude difference at the pivot scale of the P11-LS data ($L_X = 7 \times 10^{44} M_\odot$) is $\Delta \ln Y_{\text{SZ}} = 0.29$, a 3.2σ offset.

P11-X attributes the offset in their result relative to that of P11-LS to selection effects in the MCXC sample. However, we believe this interpretation is not correct for several reasons. First, the P11-X sample relied on archival data, which heavily favors X-ray selected systems. Thus, it is unclear whether the MCXC catalog is really any more “X-ray selected” than the P11-LS sample. More importantly, we emphasize that we are considering the $Y_{\text{SZ}}-L_X$ relation: that is, Y_{SZ} is considered the dependent variable. By definition, if our sample contains all galaxy clusters of a given X-ray luminosity, we can explicitly compute $\langle Y_{\text{SZ}}|L_X \rangle$ without any corrections, i.e. there are no selection effects of which to speak of. Finally, P11-X argue that the reason for the offset is a larger presence of cool-core systems in their data relative to P11-LS. We have refit the $z \in [0.13, 0.3]$ data using only cool-core systems. The resulting best fit relation is still slightly to the left of the Planck Collaboration (2011a) relation, with an amplitude offset $\Delta \ln Y_{\text{SZ}} = 0.08 \pm 0.14$. This is consistent with zero, but taken at face value, would argue that *all* galaxy clusters in Planck Collaboration (2011a) must be cool-core systems in order to account for the observed offset.

Regardless of these difficulties, we can still compare the P11-X scaling relation to our predicted V09, M10, and P11-LS($z=0.23$) $Y_{\text{SZ}}-L_X$ relations. As a simple illustrative example, Figure 8 shows as a black line the V09 prediction for the $Y_{\text{SZ}}-L_X$ scaling relation. In all cases, we find that the P11-X result is in better agreement with our predictions than the raw P11-LS data.

In short, it is not clear what drives the difference between the $Y_{\text{SZ}}-L_X$ relations of P11-X and P11-LS, nor

¹¹ To compute these regions, we used the fits from Table 4 in P11-X where both the amplitude and slope of the relation are allowed to vary. We also corrected to account for the difference between $\langle Y_{\text{SZ}}|L_X \rangle$ — the quantity measured by P11-X — and $\langle \ln Y_{\text{SZ}}|L_X \rangle$.

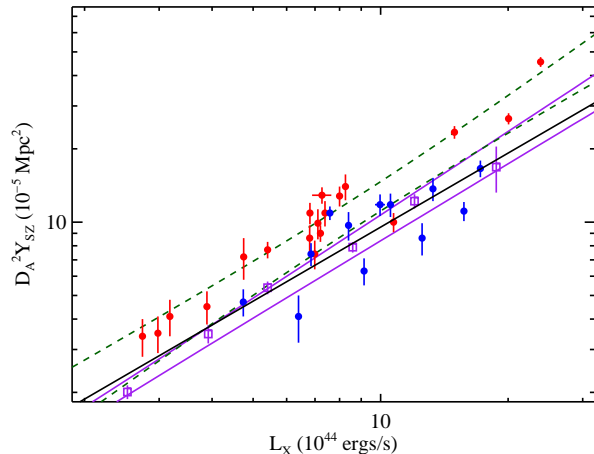


FIG. 8.— Comparison between the P11-LS (dark-green dashed lines) and P11-X (purple solid lines) fits for the $Y_{\text{SZ}}-L_X$ relation at $z = 0.23$. Both bands represent 2σ confidence intervals. Blue points are cool-core systems, while red points are not. At 2σ , the two regions barely overlap. The difference in amplitude at the pivot point of the P11-LS data ($L_X = 7 \times 10^{44}$ ergs/s) is $\Delta \ln Y_{\text{SZ}} = 0.29$, which is significant at the 3.2σ level. The black solid line is the predicted $Y_{\text{SZ}}-L_X$ relation from the V09 scaling relations, and is indicative of the excellent agreement between the predicted $Y_{\text{SZ}}-L_X$ relations and the P11-X results. The agreement of P11-X with M10 is also excellent.

which $Y_{\text{SZ}}-L_X$ scaling relations are ultimately correct. The best we can say is that all three predicted $Y_{\text{SZ}}-L_X$ scaling relations — V09, M10, and P11-LS($z=0.23$) — are viable, with better agreement found between our predictions and the P11-X results. We will return to the problem of the $Y_{\text{SZ}}-L_X$ relation in paper III.

6. COSMOLOGICAL CONSISTENCY

Having performed a detailed comparison of the cluster scaling relations from three different data sets, we test which of these relations are also consistent with the currently favored WMAP7 Λ CDM cosmological model. This test is not a priori: because of the cosmological analysis in Vikhlinin et al. (2009b) and Mantz et al. (2010a), we already know that both the V09 and M10 scaling relations are consistent with WMAP7. Here, we confirm this agreement, and test the additional L_X-M scaling relation of Pratt et al. (2009), which uses the same mass calibration as P11-LS.

We proceed as follows. We randomly sample the CMB+BAO+ H_0 Monte Carlo Markov Chains (MCMC) from Komatsu et al. (2011) for a “vanilla” flat Λ CDM cosmology. The parameters that we vary are σ_8 , n_s , Ω_m , h , and Ω_b . For each random sampling, we compute the Tinker et al. (2008) mass function. We also randomly sample the amplitude, slope, and scatter of the L_X-M relation for each of the V09, M10, and P11-LS scaling relations, and convolve the resulting mass function and $P(L_X|M)$ relations to arrive at the predicted X-ray luminosity function,

$$\frac{dn}{d \ln L} = \int d(\ln M) \frac{dn}{d \ln M} P(\ln L | \ln M). \quad (26)$$

The uncertainty in the predicted X-ray luminosity function is estimated from the variance over our Monte Carlo realizations.

We compare this prediction to the X-ray luminosity function from the REFLEX cluster survey (Böhringer et al. 2002). Note that both the reported $P(L_X|M)$ scaling relations and the REFLEX luminosity function measurement assume $\Omega_m = 0.3$ rather than the WMAP7 central value $\Omega_m = 0.27$. We do not expect this difference to be an important systematic. For instance, the difference in the luminosity distance out to $z = 0.23$ between the two models is only $\approx 0.5\%$, so we do not expect more than a few percent changes over the range of cosmologies considered here. These differences are much smaller than the relative differences between the L_X-M relations considered here.

Figure 9 shows the comparison between our predicted X-ray luminosity functions, and the REFLEX luminosity function. For our predictions, we evaluate both the mass function and L_X-M scaling relations at $z = 0.08$, the median redshift of the REFLEX clusters. The dependence of our results on the assumed redshift is mild. The bands for our theoretical predictions show the 68% confidence intervals, estimated from 10^3 random samplings of the cosmological and scaling relation parameters. The width of the REFLEX band is computed by random sampling of the Schechter luminosity function parameters L_* and α using the quoted uncertainties in Böhringer et al. (2002). In addition, it is important to note that while in our work L_X was defined using an aperture R_{500} , the REFLEX catalog defines L_X using growth curve analysis, so the two luminosities are not directly comparable. Because L_X varies very slowly with aperture, we expect that a $\pm 10\%$ systematic uncertainty in the luminosity is a reasonable estimate the impact that this difference can have. We convert this uncertainty into an uncertainty in the luminosity function using the logarithmic derivative of the average luminosity function, and add this in quadrature to the statistical error to arrive at the total uncertainty in the empirical luminosity function.

The small vertical lines along the x -axis denote the L_X corresponding to the mass pivot point of each of the three L_X-M relations. For properly calibrated scaling relations, the predicted abundance function should be statistically consistent the observed abundance at the pivot point. As expected, the V09 and M10 models are in good agreement with WMAP7, with the observed offsets significant at 0.6σ and 0.3σ respectively. The P11-LS model is in mild tension (2.1σ) with WMAP7.

We have repeated this experiment using the additional cosmological priors from the Baryon Oscillation Spectroscopic Survey (BOSS) experiment (Sanchez et al. 2012). Because the full likelihood is not yet published, we sample only the cosmological parameter $\sigma_8 \Omega_m^{1/2}$, corresponding to the standard cluster normalization condition. The cosmological prior from BOSS for this parameter is $\sigma_8 \Omega_m^{1/2} = 0.441 \pm 0.013$ (A. Sanchez, private communication). All other cosmological parameters are held fixed to their fiducial value. We have further verified that when we perform this simplified analysis on the WMAP7 results, our results are very nearly identical to the results when we allow all cosmological parameters to vary. The addition of BOSS data sharpens the previous discussion: V09 and M10 remain consistent with WMAP7+BOSS, with the abundance offset being significant at 1.5σ and 0.7σ respectively. The offset relative

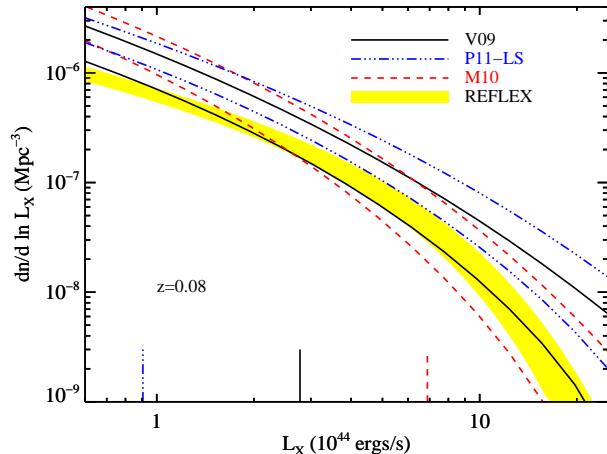


FIG. 9.— Comparison of the X-ray luminosity predicted from the L_X - M relation derived from each of the data sets to the REFLEX luminosity function, as labelled. The bands shown correspond to 68% confidence, and predictions assume a WMAP7 cosmology (Komatsu et al. 2011) sampled over σ_8 , Ω_m , h , n_s , and Ω_b . The vertical lines along the x -axis mark the pivot point of each L_X - M relation. Both V09 and M10 are consistent with cosmological expectations, while the P11-LS relation is in mild tension (2.1σ) with WMAP7. Adding BOSS priors (see text) increases the tension with P11-LS to 3.3σ , while both V09 and M10 remain consistent with the REFLEX luminosity function. Both the mass function and the scaling relations are evaluated at $z = 0.08$, the median redshift of the REFLEX catalog.

to the P11-LS prediction is 3.3σ , in modest tension with the WMAP7+BOSS results.

Interestingly, an examination of Figure 1 (L_X - M), Figure 3 (M - Y_X), Figure 4 (Y_{SZ} - Y_X), Figure 6 (Y_{SZ} - M), and Figure 7 (Y_{SZ} - L_X), reveal that at the pivot point of the M10 data set, the amplitude of the V09 scaling relations are in good agreement with the amplitude of the M10 scaling relations. That is, the V09 and M10 relations are in good agreement for the most massive clusters, but diverge at low masses because of the differences in the $f_{\text{gas}}-M$ relation between the two works. From Figure 9, we see that the f_{gas} model of V09 is a better match to the full set of scales probed by REFLEX. This stands in contrast to the results of Allen et al. (2008). However, the latter work focused on the most massive galaxy clusters in the Universe, so the two results may be reconciled if there is a flattening of the slope in the $f_{\text{gas}}-M$ relation at the highest masses.

7. SUMMARY AND CONCLUSIONS

We have performed a detailed comparison of the X-ray scaling relations from three different data sets: P11-LS (Pratt et al. 2009; Arnaud et al. 2010; Planck Collaboration 2011b), V09 (Vikhlinin et al. 2009a; Roza et al. 2012a), and M10 (Mantz et al. 2010b). We compare the L_X - M , M - Y_X , and Y_{SZ} - Y_X scaling relations and find varying degrees of tension between the works. Differences are partly traced to the systematic offsets in cluster observables characterized in paper I, but the constant f_{gas} model of M10 drives slope differences relative to V09 and P11-LS. After correcting for these two effects, all cluster scaling relations are in good agreement with each other. Indeed, at the pivot point of the M10 scaling relations, all of the V09 and M10 scal-

ing relations are in good agreement with each other: the difference between these two works is pronounced only if one extrapolates the M10 scaling relations to low mass systems.

Having identified the sources of tension, we use these scaling relations to self-consistently recover the Y_{SZ} - M and Y_{SZ} - L_X scaling relations within the context of a multivariate Gaussian model for cluster properties (see Appendix A, also White et al. 2010). In the limit of very small scatter, the transfer relations are equivalent to “plugging-in” one relation into another. In the presence of finite scatter, there are additional terms involving property covariance and the local slope of the mass function that must be taken into account. For instance, in the case of the Y_{SZ} - L_X scaling relation, these corrections are of order 25%.

The differences in mass calibration between the various data sets, presented in paper I, lead to different predictions for the Y_{SZ} - M scaling relation. Independent results from the LoCuSS collaboration (Marrone et al. 2011) are not yet able to distinguish between the various predictions.

For Y_{SZ} - L_X scaling, we find that the differences between the various data sets are moderate. Indeed, we compared each of the predicted Y_{SZ} - L_X scaling relations to the P11-LS data, and found reasonable agreement in all cases. We also compared our predicted Y_{SZ} - L_X scaling relations with those of Planck Collaboration (2011a, referred to as P11-X), noting that there are large differences between the P11-LS and the P11-X results (4.1σ significance), finding much better agreement with the P11-X results for the V09 and M10 data sets. The selection effects required to reconcile the P11-LS and P11-X would have to be large, with the MCXC catalog comprised exclusively of cool-core clusters, or SZ selection leading to an observed 30% amplitude shift; either solution seems too large to be plausible, as correction terms from selection effects in SZ typically scale as the variance $\sigma_{sz|m}^2 \approx 0.01$, where as the observed offset is nearly 30% in Y_{SZ} .

Finally, we consider whether the scaling relations from each of the three data sets are consistent with cosmological expectations. We convolve the three L_X - M relations with the mass function predicted by a WMAP7 cosmology — sampling over σ_8 , Ω_m , n_s , h , and Ω_b — and compare these predictions against the observed REFLEX luminosity function (Böhringer et al. 2002). As expected, the M10 and V09 scaling relations are consistent with the REFLEX luminosity function at the pivot point of the two samples. The prediction from the P11-LS L_X - M scaling relation is offset from the REFLEX data by 2.1σ . Adding BOSS priors increases the tension with P11-LS to 3.3σ , while both the V09 and M10 predictions remain consistent with the data. In addition, comparing the M10 and V09 predictions, it is clear that the abundance of low mass systems is correctly predicted by V09 but not by M10, which argues that an f_{gas} model $f_{\text{gas}} \propto M^\gamma$ with $\gamma \approx 0.10 - 0.15$ is a better match to the data over the full range of scales probed by REFLEX galaxy clusters. Because f_{gas} is observed to be constant at high masses (Allen et al. 2008), this may be signaling a steepening of the $f_{\text{gas}}-M$ relation at low masses.

The fact that the three different X-ray data sets con-

sidered here and in paper I exhibit systematic differences in mass calibration and cluster scaling relations has important consequences for the predictions of the $Y_{\text{SZ}}-N_{200}$ scaling relation for optical galaxy clusters in Planck Collaboration (2011c). In particular, the fact that the different data sets give rise to different $Y_{\text{SZ}}-M$ scaling relations also implies that the predicted $Y_{\text{SZ}}-N_{200}$ relations from each of these data sets will be different. In paper III, we explore whether any of these three data sets can resolve this issue, and whether doing so results in a self-consistent picture of multi-variate cluster scaling relations. More specifically, we will demand not just that the predicted $Y_{\text{SZ}}-N_{200}$ relation match observations, but also that any two scaling relations can be combined to successfully predict the third, while simultaneously satisfying cosmological expectations for the counts of galaxy clusters selected by any property.

The authors would like to thank Adam Mantz, Alexey Vikhlinin, Gabriel Pratt, Monique Arnaud, and Steven

Allen for useful criticisms on earlier drafts of this work. The authors would also like to thank the organizers of the Monsters Inc. workshop at KITP, supported in part by the National Science Foundation under Grant No. PHY05-51164, where this collaboration was started. ER gratefully acknowledges the hospitality of the AstroParticle and Cosmology laboratory (APC) at the Université Paris Diderot, where part of this work took place. ER is funded by NASA through the Einstein Fellowship Program, grant PF9-00068. AEE acknowledges support from NSF AST-0708150 and NASA NNX07AN58G. JGB gratefully acknowledges support from the Institut Universitaire de France. A portion of the research described in this paper was carried out at the Jet Propulsion Laboratory, California Institute of Technology, under a contract with the National Aeronautics and Space Administration. This work was supported in part by the U.S. Department of Energy contract to SLAC no. DE-AC02-76SF00515.

REFERENCES

- Allen, S. W., Evrard, A. E., & Mantz, A. B. 2011, ArXiv:1103.4829
 Allen, S. W. et al. 2008, MNRAS, 383, 879
 Andreon, S. & Hurn, M. A. 2010, MNRAS, 404, 1922
 Angulo, R. E. et al. 2012, ArXiv:1203.3216
 Arnaud, M., Pointecouteau, E., & Pratt, G. W. 2007, A&A, 474, L37
 Arnaud, M. et al. 2010, A&A, 517, A92+
 Battaglia, N. et al. 2011, ArXiv: 1109.3709
 Biesiadzinski, T. et al. 2012, ArXiv:1201.1282B
 Böhringer, H., Dolag, K., & Chon, G. 2012, A&A, 539, A120
 Böhringer, H. et al. 2002, ApJ, 566, 93
 —. 2004, A&A, 425, 367
 Eckmiller, H. J., Hudson, D. S., & Reiprich, T. H. 2011, A&A, 535, A105
 Fabian, A. C. et al. 1994, MNRAS, 267, 779
 Fabjan, D. et al. 2011, MNRAS, 416, 801
 Hartley, W. G. et al. 2008, MNRAS, 386, 2015
 Henry, J. P. et al. 2009, ApJ, 691, 1307
 Kaiser, N. 1986, MNRAS, 222, 323
 Kay, S. T. et al. 2012, MNRAS, 2792
 Koester, B. et al. 2007, ApJ, 660, 239
 Komatsu, E. et al. 2011, ApJS, 192, 18
 Krause, E. et al. 2012, MNRAS, 419, 1766
 Kravtsov, A. V., Vikhlinin, A., & Nagai, D. 2006, ApJ, 650, 128
 Magliocchetti, M. & Brügggen, M. 2007, MNRAS, 379, 260
 Mantz, A. et al. 2010a, MNRAS, 406, 1759
 —. 2010b, MNRAS, 406, 1773
 Marrone, D. P. et al. 2011, ArXiv:1107.5115
 Maughan, B. J. et al. 2012, MNRAS, 421, 1583
 Mittal, R. et al. 2011, A&A, 532, A133
 Nagai, D. 2006, ApJ, 650, 538
 Nagai, D., Kravtsov, A. V., & Vikhlinin, A. 2007, ApJ, 668, 1
 Noh, Y. & Cohn, J. D. 2011, MNRAS, 158
 —. 2012, ArXiv:1204.1577
 Okabe, N. et al. 2010, PASJ, 62, 811
 Piffaretti, R. et al. 2011, A&A, 534, A109
 Planck Collaboration. 2011a, A&A, 536, A10
 —. 2011b, A&A, 536, A11
 —. 2011c, A&A, 536, A12
 —. 2012, ArXiv:1204.2743
 Pointecouteau, E., Arnaud, M., & Pratt, G. W. 2005, A&A, 435, 1
 Pratt, G. W. et al. 2009, A&A, 498, 361
 Rasia, E. et al. 2011, ApJ, 729, 45
 Rowley, D. R., Thomas, P. A., & Kay, S. T. 2004, MNRAS, 352, 508
 Rozo, E., Vikhlinin, A., & More, S. 2012a, ArXiv:1202.2150
 Rozo, E. et al. 2009, ApJ, 699, 768
 —. 2010, ApJ, 708, 645
 —. 2012b, In preparation
 Sanchez, A. G. et al. 2012, ArXiv:1203.6616
 Short, C. J. et al. 2010, MNRAS, 408, 2213
 Stanek, R. et al. 2010, ApJ, 715, 1508
 Tinker, J. et al. 2008, ApJ, 688, 709
 Vikhlinin, A. et al. 2006, ApJ, 640, 691
 —. 2009a, ApJ, 692, 1033
 —. 2009b, ApJ, 692, 1060
 White, M., Cohn, J. D., & Smit, R. 2010, MNRAS, 408, 1818

APPENDIX

A LOCAL MODEL FOR MULTI-VARIATE SCALING RELATIONS

We consider the problem of a locally power-law halo mass function $dn/d\ln M \propto M^{-\beta}$, and a vector of observable signals \mathbf{S} , e.g. $\mathbf{S} = \{L_X, Y_X, M_{\text{gas}}, Y_{\text{SZ}}, \text{etc.}\}$. The results summarized here are an extension of those presented in Stanek et al. (2010) and Allen et al. (2011), and are basically equivalent to those in Appendix C of White et al. (2010). We define $\mu = \ln(M/M_0)$ and $s = \ln(S_i/S_{i,\text{ref}})$ where M_0 and $S_{i,\text{ref}}$ represent a choice of units. The scaling relations between \mathbf{S} and M are governed by the probability distribution $P(\mathbf{s}|\mu)$ which we assume to be Gaussian. The means of the distributions are parameterized as

$$\langle \mathbf{s} | \mu \rangle = \mathbf{a} + \boldsymbol{\alpha} \mu. \quad (\text{A1})$$

The scatter is characterized by a covariance matrix, C , which has the property variance, σ_i^2 , along the diagonals and off-diagonal terms, $C_{ij} = \langle (s_i - \langle s_i \rangle)(s_j - \langle s_j \rangle) \rangle$. The correlation coefficient, given by $r_{ij} = C_{ij}/\sigma_i\sigma_j$, lies between -1 and 1 .

Using Bayes Theorem, we can relate the \mathbf{S} - M scaling relation to the M - \mathbf{S} scaling relation

$$P(\mu|\mathbf{s}) = \frac{P(\mathbf{s}|\mu)P(\mu)}{P(\mathbf{s})} = \frac{P(\mathbf{s}|\mu)P(\mu)}{\int d\mu P(\mu)P(\mathbf{s}|\mu)}. \quad (\text{A2})$$

For a locally power-law model, $P(\mu) \propto \exp(-\beta\mu)$, the resulting probability density is Gaussian with mean and variance

$$\langle \mu|\mathbf{s} \rangle = \boldsymbol{\alpha} \mathbf{C}^{-1} (\mathbf{s} - \mathbf{a}) \sigma_{\mu|\mathbf{s}}^2 - \beta \sigma_{\mu|\mathbf{s}}^2 \quad (\text{A3})$$

$$\sigma_{\mu|\mathbf{s}}^2 = (\boldsymbol{\alpha} \mathbf{C}^{-1} \boldsymbol{\alpha})^{-1} \quad (\text{A4})$$

For a single property, s , the above expressions reduce to

$$\langle m|s \rangle = \frac{s - a}{\alpha} - \beta \sigma_{\mu}^2, \quad (\text{A5})$$

$$\sigma_{\mu} = \frac{1}{\alpha} \sigma_s. \quad (\text{A6})$$

The correction term to the mean mass, $-\beta\sigma_{\mu}^2$, is the standard Malmquist bias correction. Here, σ_{μ} is the scatter in halo mass of a sample selected by property s .

The space density of clusters with multiple properties, \mathbf{s} , is

$$n(\mathbf{s}) = \int d\mu P(\mathbf{s}|\mu)n(\mu) = \frac{A\sigma_{m|\mathbf{s}}}{(2\pi)^{(N-1)/2}|\mathbf{C}|^{1/2}} \exp \left[-\frac{1}{2} \left((\mathbf{s} - \mathbf{a}) \mathbf{C}^{-1} (\mathbf{s} - \mathbf{a}) - \frac{\langle m|\mathbf{s} \rangle}{\sigma_{\mu|\mathbf{s}}^2} \right) \right]. \quad (\text{A7})$$

In the case of a single signal s , this reduces to

$$n(s) = \frac{A}{\alpha} \exp \left[-\beta \left(\frac{s - a}{\alpha} - \frac{1}{2} \beta \sigma_{\mu}^2 \right) \right]. \quad (\text{A8})$$

Note the slope of the abundance function is simply β/α , as we would expect. There is a correction term to the amplitude, $\beta^2\sigma^2$, which reflects the number boost due to low mass halos scattered upward.

Of particular interest to us is the case in which there are two signals s_1 and s_2 . Let $\sigma_{\mu 1}$ and $\sigma_{\mu 2}$ be the mass scatter in each, respectively. Then the mean selected mass, $\langle \mu|\mathbf{s} \rangle$, and the mass variance for joint signals, s_1 and s_2 , are

$$\langle \mu|s_1, s_2 \rangle = \frac{\sigma_{\mu 1}^{-2} \alpha_1^{-1} (s_1 - a_1) + \sigma_{\mu 2}^{-2} \alpha_2^{-1} (s_2 - a_2) - r \sigma_{\mu 1}^{-1} \sigma_{\mu 2}^{-1} (\alpha_1^{-1} (s_1 - a_1) + \alpha_2^{-1} (s_2 - a_2))}{\sigma_{\mu 1}^{-2} + \sigma_{\mu 2}^{-2} - 2r \sigma_{\mu 1}^{-1} \sigma_{\mu 2}^{-1}} \quad (\text{A9})$$

$$\sigma_{\mu|\mathbf{s}}^2 = \frac{1 - r^2}{\sigma_{\mu 1}^{-2} + \sigma_{\mu 2}^{-2} - 2r \sigma_{\mu 1}^{-1} \sigma_{\mu 2}^{-1}}. \quad (\text{A10})$$

Finally, a further application of Bayes theorem allows us estimate $P(s_2|s_1)$,

$$P(s_2|s_1) = P(s_1, s_2) \frac{1}{P(s_1)} = \frac{1}{P(s_1)} \int dm P(s_1, s_2|\mu)P(\mu) \quad (\text{A11})$$

from which we find that $P(s_2|s_1)$ is a Gaussian distribution with mean and variance

$$\langle s_2|s_1 \rangle = a_{2|m} + \alpha_2 (\langle \mu|s_1 \rangle + r \beta \sigma_{\mu 1} \sigma_{\mu 2}) \quad (\text{A12})$$

$$\sigma_{2|1}^2 = \alpha_2^2 [\sigma_{\mu 1}^2 + \sigma_{\mu 2}^2 - 2r \sigma_{\mu 1} \sigma_{\mu 2}] \quad (\text{A13})$$

The correlation coefficient between s_2 and m at fixed s_1 is given by

$$r_{2,\mu|1} = \frac{\sigma_{\mu 1} / \sigma_{\mu 2} - r}{[1 - r^2 + (\sigma_{\mu 1} / \sigma_{\mu 2} - r)^2]^{1/2}}. \quad (\text{A14})$$

LIKELIHOOD PLOTS

Figures 10 and 11 show the posterior distribution for the $Y_{\text{SZ}}-M$ and $Y_{\text{SZ}}-L_X$ scaling relation parameters summarized in Table 3.

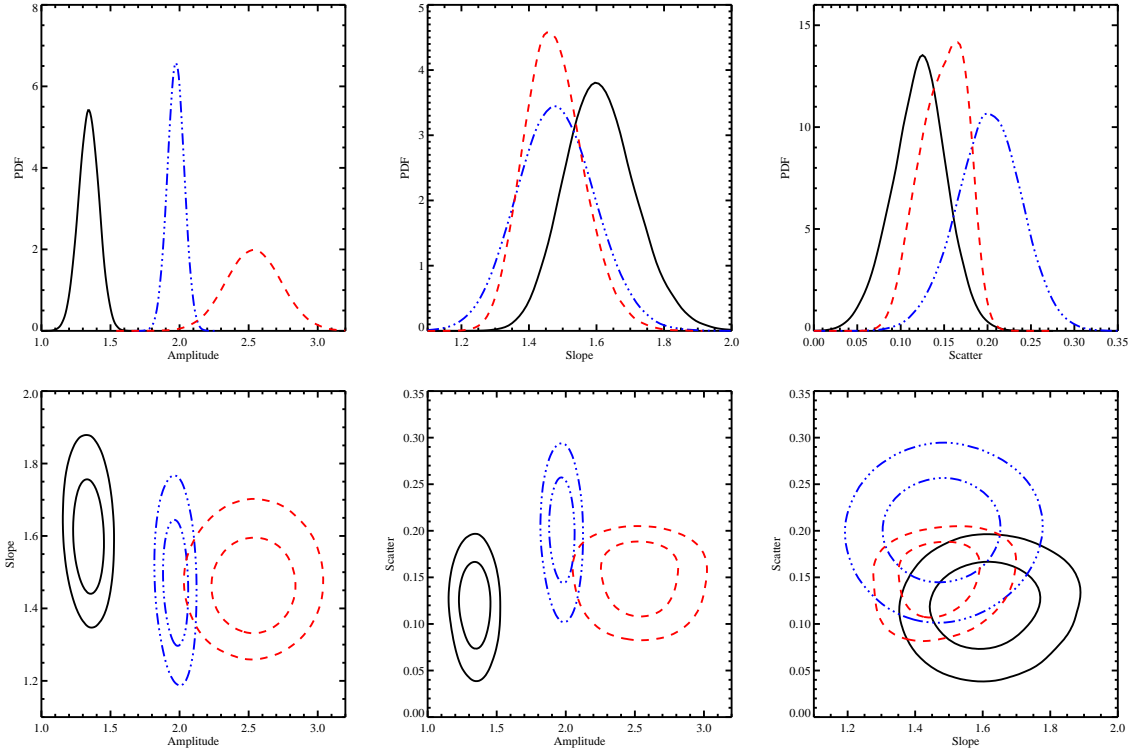


FIG. 10.— Likelihood distribution and likelihood contours for the parameters of the $Y_{SZ}-M$ scaling relation. Black solid=V09, blue dash-dot=P11-LS($z=0.23$), and red dashed=M10. All contours are 68% and 95% confidence. Note the different pivot points, so one cannot directly compare the amplitudes quoted between all data sets.

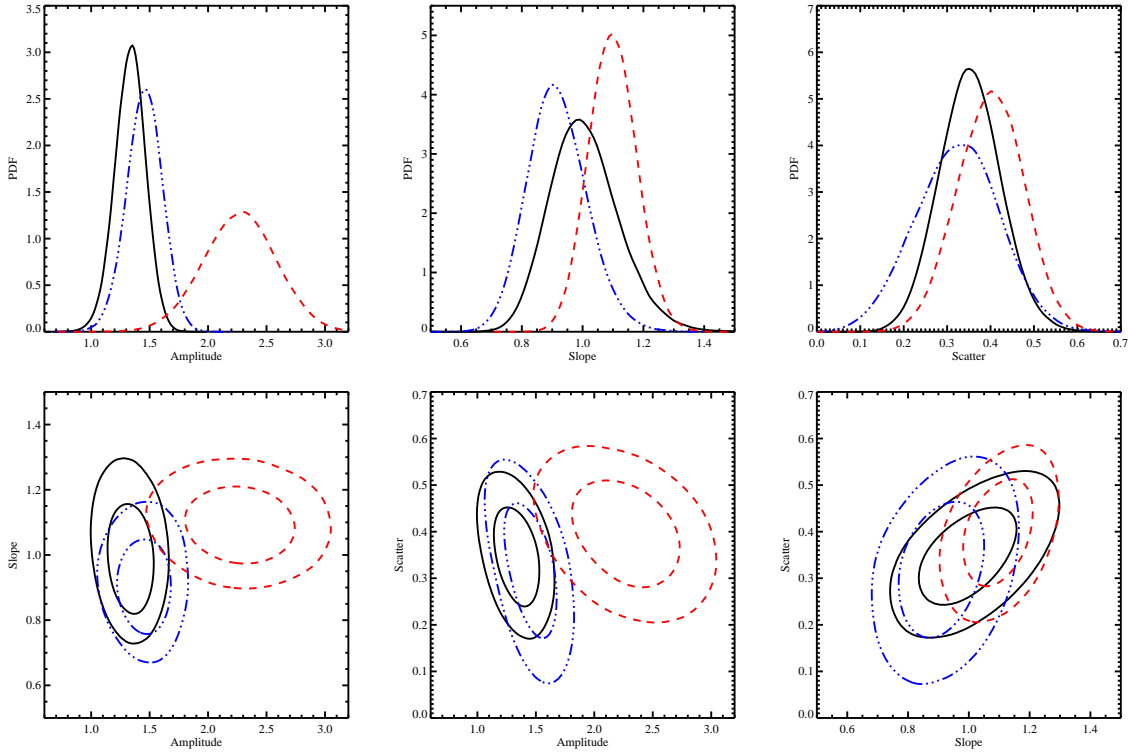


FIG. 11.— As Figure 10, but for the $Y_{SZ}-L_X$ parameters.